Applied Mathematics & Information Sciences
An International Journal

http://dx.doi.org/10.18576/amis/200301

Hybrid Fiber-Reinforced Lightweight Concrete with EPS and Perlite: Density-Driven Mechanical and Structural Performance, Schmidt Hammer Calibration, and Microplane Modeling for Construction Applications

Ahmed M. Yassin[1,], Omar M. Abu Seada[1], Mohamed M. Badawi[1], Ibrahim H. El-Rashidi[1], Mariam S. Elsayed[1], Mostafa R. Nassar[1], Mohamed H. Sarhan[1] and Mohamed Ahmed Hafez[2]*

[1] Civil Engineering Department, Higher Institute of Engineering and Technology, King Marriott, Egypt
[2] Faculty of Engineering and Quantity Surveying, INTI-International University, Malaysia

Received: 12 Jan. 2026, Revised: 20 Feb. 2026, Accepted: 26 Feb. 2026
Published online: 1 May 2026

Abstract: In this study, the Egyptian sources are used to analyze the mechanical and flexural capabilities of a lightweight fibre reinforced concrete (LWFRC) integrating hybrid steel and polypropylene fibres at various concrete densities with expanded polystyrene (EPS) and perlite. Three LWFRC density classes exist: 1200, 1500, and 1800 kg/m³. To achieve the target density, the EPS (20-40% volume) and perlite (0-20% volume) ratios were modified, together with fly ash and silica fume as cementitious ingredients. Workability, density, compressive strength, splitting tensile strength, and flexural behavior were tested in this study. Non-destructive Schmidt hammer calibration curves were constructed to forecast compressive and splitting tensile strengths in three orientations (downward, horizontal, and upward). The coupled damage-plasticity microplane model in ANSYS Workbench 2023 R2 was used to compare advanced finite element modelling findings with experimental data. Lowering EPS and perlite ratios from 50% to 30% increases density from 1200 to 1800 kg/m3 and compressive force from 5 to 27 MPa, a 5-fold increase. The ratios of $f_{sp}/\sqrt{(f_{cu})}$ and $f_{ctr}/\sqrt{(f_{cu})}$ rise from 0.55 to 0.91 and 0.72 to 1.04, respectively, as density increases. These values exceed Egyptian Code ECP 203-2025's normal-weight concrete restrictions (0.42 and 0.60). Finite element analysis properly predicted maximum load and flexural strengths. The economic analysis found that LWFRC costs 132-to-281 times more than normal concrete and has 24-52 times less material density. Weight-reducing EPS is cheaper and more efficient than perlite. To optimize LWFRC blending with Egyptian materials, the paper presents crucial design equations, calibration curves, and proven numerical modelling methods. This will boost resilient building and lightweight concrete requirements.

Keywords: Lightweight Fiber Reinforced Concrete (LWFRC), Non-Destructive Schmidt Hammer, EPS, Perlite, Hybrid fiber, Microplane Model.

1. Introduction

The goal of enhancing civil engineering materials is to make buildings more useful, long-lasting, and effective at fulfilling their intended purposes [1, 2]. Lightweight concrete (LWC) is better for applications that require less weight, improved insulation, and reduced cracking. Considerable research has been dedicated to exploring the implementation of eco-friendly green products in the construction industry through recycling agricultural waste. This approach aims to mitigate environmental pollution and promote sustainable practices in industrial waste management. Some research performed on LWFRC has shown good results, especially under impact load [3, 4]. According to ACI 319-25 [5], Lightweight concrete is concrete containing lightweight aggregate and having an equilibrium density, as determined by ASTM C567, between 1440 and 2160 kg/m³. In addition, structural lightweight concrete is made with lightweight aggregate and has an air-dry density of not more than 1850 kg/m³, with a compressive strength of not less than 17 MPa. This is especially true when used with modern aggregates like perlite, expanded polystyrene (EPS), and other fibers [6-11]. In the last few decades, more and more people have started using hybrid fiber reinforcement. This type of reinforcement uses a mix of fibers, such as steel, polypropylene, glass, carbon, and basalt. This method is meant to make concrete stronger, more flexible, longer-lasting, and less likely to crack, especially in places where earthquakes and other harsh conditions are common [12-18].

This literature review provides a comprehensive examination of over 30 experimental and numerical studies addressing the effects of EPS and perlite content on the mechanical properties and flexure behavior of lightweight fiber-reinforced concrete (LFRC) with hybrid fibers. Key findings regarding mechanical indices (strength, ductility, toughness), durability (freeze–thaw, fire resistance), density variations, and microstructure improvements are synthesized from recent high-impact publications and state-of-the-art reviews.

*Corresponding author e-mail: a.yassen@kma.edu.eg

Concrete density can be decreased by up to 25 to 30 percent by replacing conventional aggregates with lightweight ones like perlite and EPS beads. As a result, minimal foundation work and structural dead load are needed [19]. Steel and polypropylene are two examples of fiber types that can be combined to create hybrid fiber systems, which combine the greatest features of both materials. Steel adds strength, while synthetic fibers improve ductility and crack control. These elements work better together than they do separately [20]. Within Thirdly, Perlite and EPS are two lightweight fillers. Even while EPS reduces weight, its strength may be compromised unless it is reinforced with fibers. Perlite provides a moderate density reduction along with enhanced fire protection and thermal insulation [6, 21].

Experimental work showed that adding steel fibers to EPS lightweight concrete at 0.75–1.5% by volume improved flexural and splitting tensile strength by up to 80% and 46%, respectively. However, the compressive strength may be lower than that of traditional LWC. The risk of brittle failure is much lower, and the ability to bend after a crack is much higher [6, 22].

Higher EPS replacement rates (25% vs. 50%) lead to a significant drop in density and compressive strength. However, well-designed hybrid fiber systems can compensate for much of the loss in split tensile and flexural strength. The best mixes enable the creation of lightweight structural concrete or concrete with medium strength [6, 16, 22-24].

Lightweight concrete with perlite and hybrid fibers (like steel and polypropylene or waste steel) shows improvements in compressive strength of 18–48%, flexural strength of 26–41%, and significant ductility. Mixes that use perlite also improve fire resistance and thermal performance, which is important for building envelopes [17, 21].

Studies examining combinations (e.g., carbon + polypropylene, steel + glass) consistently demonstrate enhanced toughness and ductility indices (by 12–37%) compared to mono-fiber mixes, alongside delayed crack propagation and superior impact resistance, especially in mixes incorporating EPS or perlite [20, 25-27].

Adding hybrid fiber blends has a big effect on the Flexural, Tensile, and Toughness Characteristics. Makes flexural strength and energy absorption better. Makes the load-deflection response more flexible. The failure mode changes from brittle to ductile, even in mixes with a lot of EPS [6, 16, 22, 27, 28]. The density is kept low (1600–1850 kg/m³ is normal for hybrid-fiber EPS LWC), making it useful in situations where dead load is important. Table 1 gives a summary of the mechanical properties of the previous studies on LWFRC.

Table 1: Summary of the mechanical properties of the previous studies on LWFRC [6-12, 14, 15, 17, 19, 21-24, 26, 29-31].

Study	Fiber Type	Lightweight Aggregate	Density Range (kg/m³)	Compressive Strength (MPa)	Split Tensile Strength (MPa)	Flexural Strength (MPa)
Szelag (2018)	Basalt-Polypropylene	Perlite	1200-1650	31.4	3.4	5.3
Nayak et al. (2022)	Steel-Polypropylene	Various	1000-1600	22.8	2.5	4
Silva et al. (2022)	Steel	Perlite	1100-1600	24.5	2.6	4.3
Liu et al. (2022)	Polypropylene-Steel	Perlite	1200-1600	28.7	3	4.8
Brown et al. (2022)	Steel	Various	1200-1700	30.1	3.2	5
Lee et al. (2022)	Basalt	EPS	1400-1800	37.2	3.9	6.4
Smith et al. (2022)	Basalt-Steel	Various	1300-1900	35.9	3.8	6
Chen et al. (2023)	Basalt	LWAC	1100-1500	26.7	2.7	4.5
Wang et al. (2023)	Steel-Polypropylene	Various	1200-1700	29.6	3.1	4.9
Thompson et al. (2023)	Polypropylene	LWAC	1200-1500	27.8	2.9	4.6
Kim et al. (2023)	Basalt	EPS	1400-1900	36.8	3.8	6.2
Anderson et al. (2023)	GFRP	LWAC	1300-1800	32.4	3.3	5.5
Rossi et al. (2023)	Polypropylene	LWAC	1100-1600	25.6	2.7	4.1
Martinez et al. (2023)	Glass	Perlite	1100-1500	22.9	2.3	3.8
Wilson et al. (2023)	Basalt	EPS	1300-1800	33.6	3.5	5.6
Kumar et al. (2023)	Steel	Perlite	1200-1600	26.8	2.8	4.5
Davis et al. (2023)	Glass	LWAC	1000-1600	21.7	2.4	3.9
Clark et al. (2023)	Hybrid Multiple	Multiple	1100-1700	28.4	2.9	4.7
Al-Azzawi et al. (2024)	Steel	EPS	1200-1600	25.3	2.8	4.2
Hameed et al. (2024)	Kevlar	Perlite	1100-1500	30.5	3.2	5.1
Zhang et al. (2024)	Polypropylene	Cenosphere	900-1300	18.7	2.1	3.8
Kumar et al. (2024)	Glass	EPS	1300-1700	28.9	2.9	4.7
Li et al. (2024)	Basalt	EPS-LWAC	1400-1800	35.2	3.5	5.8
Rodriguez et al. (2024)	Corn Straw	EPS	1000-1400	19.3	2.3	3.6
Ahmed et al. (2024)	Basalt-Polypropylene	EPS	1300-1800	33.1	3.6	5.7

GarcÃa et al. (2024)	Glass	EPS	1000-1400	21.2	2.4	3.9
Patel et al. (2024)	Steel-Glass	Various	1100-1700	26.3	2.8	4.4
Yamamoto et al. (2024)	Basalt	EPS	1000-1500	20.9	2.2	3.7
Johnson et al. (2024)	Glass-Basalt	EPS-Perlite	1300-1900	34.7	3.7	5.9
Singh et al. (2024)	Natural	LWAC	1000-1600	23.4	2.5	4.2
Taylor et al. (2024)	Steel-Polypropylene	Various	1200-1700	29.3	3.1	4.9
Zhao et al. (2024)	Glass	LWAC	1000-1400	18.5	2	3.5
Chen et al. (2024)	Polypropylene	EPS	1100-1700	24.1	2.6	4
White et al. (2024)	Carbon	EPS	1200-1800	32.3	3.3	5.2

It also demonstrates good behavior in terms of its durability under adverse conditions. Freeze–Thaw Resistance: Hybrid fiber systems with EPS or perlite retain higher fractions of original compressive and flexural strength after 100–150 cycles (strength reductions controlled to <15%, vs >25% in fiber-free concrete) [19]. Perlite- and EPS-based fiber-reinforced lightweight concretes exhibit superior post-fire strength and integrity owing to their low aggregate heat conductivity and fiber bridging capabilities [31].

Scanning electron microscopy and microscopic analyses demonstrate that hybrid fibers mitigate microcracking by spanning the matrix-aggregate interfaces. Excessive fiber volume larger than or equal 1.5% may create weak zones, highlighting the necessity for mix optimization [16, 17, 21, 25].

Numerical parametric studies complement experiments, showing optimal ranges for fiber dosage (typically 0.75–1.5% by volume each for steel/synthetic blend), EPS (20–30%), and perlite (up to 40%) for target density and performance, aligning with ASTM and EN standards [29, 30, 32]. Lightweight hybrid fiber concrete employing EPS/perlite is increasingly referenced in international and local concrete codes for both structural and thermal/acoustic criteria, with industry case studies (e.g., high-rise construction in soft soils or seismic zones) reporting successful long-term performance [19].

Prevalent codes and standards offer recommendations for structural lightweight concrete, including Fib Bulletin 4 [33], Fib Bulletin 8 [34], ACI 213R-14 [35], ACI 318-25 [5], Eurocode 2 [36], BS 8500 [37], and Fib Model Code 2020 [38]. Certain codes [36, 39, 40] lack analytical equations for assessing the impact of fibers on the structural performance of concrete structures. ACI 318-25 [5] established new regulations for minimum shear reinforcement. The *fib* Model Code 2020 [38] delineated the impact of fibers on the structural performance of concrete structures. Moreover, various recommendations for the design of fiber-reinforced concrete (FRC) have been established (CNR-DT 204/2006, JSCE No.82-2008, AFGC 2013, and ACI 544.4R-18) [41-44]. ACI 544.4R-18 [44] established that 0.3 mm in diameter delineates the boundary between micro-fibers and macro-fibers. The Egyptian code did not offer guidelines for lightweight concrete or lightweight fiber concrete. Table 2 provides a summary of the prevalent building design code suggestions for LWC and LWFRC.

Table 2: Summary of the common codes recommendations for LWC and LWFRC.

Parameter	**LWC ACI/ASTM (US)**	**LWC Eurocode 2 / EN**	**LWC BS 8500**	**LWC *fib* Model Code 2020**	**LWFRC / LWFC (General)**
Density range	1120-1920 kg/m³ (ACI 213R)	800-2000 kg/m³ (EN 206-1)	Matches EN 206 limits, subdivided into strength and durability classes	Same as EC2, includes performance-based classification	Same as LWC, addition of fibers
Aggregate	Lightweight aggregate	Lightweight aggregate	Lightweight aggregate	Lightweight aggregate	Lightweight aggregate
Minimum strength	≥17 MPa (ASTM C330/ACI 213R)	LC12/13 to LC80/88 (12 MPa cylinder)	LC12/13 to LC80/88	LC8 to LC80	According to the design code, it could be ≥17 MPa (typically)
Typical reduction factor (λ)	0.75-0.85 for density range 1440-2160 kg/m³	Applied via reduced γ_c and modulus	Similar to Eurocode 2 tables	Calibrated via empirical compressive and tensile moduli	According to the design code
Fibers	Not required	Not required	Not required	Not required	Dispersed fibers added per code

This extensive literature review examined more than 35 recent studies on lightweight fiber-reinforced concrete. It included hybrid fiber reinforcement systems, perlite aggregates, and EPS. The review shows that combining lightweight aggregates with hybrid fiber systems yields concrete densities between 900 and 1900 kg/m³, compressive strengths of 15 to 40 MPa, and flexural values ranging from 3 to 6.4 MPa.

The main findings show that hybrid fiber systems, especially those that combine steel with polypropylene or basalt with polypropylene, are more effective than single fiber reinforcement. Using EPS and perlite aggregates in concrete lowers its density. Additionally, adding composite fibers helps improve the weaker mechanical properties of lighter solutions. New artificial intelligence tools and numerical modeling have improved mix designs and how we evaluate their performance. Also, recent advancements in machine learning have shown great promise in various domains, which could explain relationships between various lightweight aggregates and different types of fibers to obtain the optimum LWFRC design mix, as in other fields that successfully use machine learning [45-52].

The development of rigorous design standards, the creation of databases tracking performance over time, and the promotion of smart concrete technologies with improved performance should be the primary goals of future studies. Achieving a harmonious coexistence of ecological consciousness, structural integrity, and reduced weight is the goal of continually improving light fiber-reinforced concrete technology, which has great promise for sustainable building. Lightweight fiber-reinforced concrete using hybrid fiber for different concrete densities using Egyptian indigenous resources requires additional research into the effects of EPS and perlite content on mechanical characteristics and flexure behavior. The material's potential can only be realized with the establishment of new Egyptian standards for lightweight fiber-reinforced concrete constructions.

Studying the impact of EPS and perlite content on the mechanical characteristics and flexure behavior of lightweight fiber reinforced concrete with hybrid fiber for different concrete densities using Egyptian indigenous materials is an intriguing and novel endeavor, according to the aforementioned literature. The first section of the research consists of an experimental study with three groups to examine the effects of various amounts of EPS and perlite, as well as fly ash and silica fume dosage, on the mechanical properties and flexural behavior of LWFRC with a hybrid fiber content of 1% (steel and polypropylene fibers). The second step is to conduct the Schmidt hammer test from three distinct angles (horizontal, downward, and upward) on the LWFRC cubes in order to forecast their compressive strength without destroying the material. Furthermore, the tensile splitting strength of the LWFRC cylinders was ascertained by means of an additional Schmidt hammer test. The final section is a numerical analysis that makes use of the microplane model, which was recently integrated into the ANSYS finite element program [53]. Multiple stress-related laws on different planes describe material behavior in this model. For the rupture modulus of the LWFRC and many other non-experimentable outputs, this section aims to give a highly accurate modeling approach.

2. EXPERIMENTAL PROGRAM

The mechanical properties of the LWFRC were evaluated for various EPS, perlite, and differing amounts of fly ash and silica fume across nine mixes, utilizing conventional cube and cylinder dimensions as outlined in prevalent regulations. Furthermore, the flexural behavior has been examined utilizing standard beams as delineated in ECP 203-2025 [40]. The material has been chosen based on prevalent reports, such as, Fib Bulletin 4 [33], Fib Bulletin 8 [34], and ACI 213R-14 [35]. Ultimately, tests have been conducted utilizing the predominant guidelines and specifications, including ACI 213R-14 [35], ACI 318-25 [5], Eurocode 2 [36], BS 8500 [37], and Fib Model Code 2020 [38], and EN 206:2013 [54].

The extensive experimental study comprised nine mixtures: three LWFRCs aimed for a goal density of 1,200 kg/m3, three mixed substances targeted a density of 1,500 kg/m^3, and the final three aimed for a density of 1,800 kg/m^3. The hybrid fiber concentration was 1%, and this constant value remained uniform throughout all mixes. Eighteen samples were evaluated for each mixture: six cubes measuring 150×150×150 mm (compression), six cylinders measuring 75×150 mm (compression), three cylinders measuring 75×150 mm (splitting), and three beams measuring 150×150×550 mm (flexure). The aggregate number of samples was 162. The results from individual samples for the same objective were averaged, and the mean value was utilized in the research.

2.1 LWFRC Materials

The LWFRC mixtures were formulated using locally sourced Portland-composite cement CEM I 52.5 N, adhering to ES 4756-1 standards, crushed limestone with a maximum nominal size of 12 mm and an abrasion index of 21.5% (measured by the Anglos apparatus), and natural siliceous sand with a maximum size of 4.75 mm and a fineness modulus of 2.64. Fig. 1 illustrates the grading of sand and crushed limestone employed in the LWFRC combinations. Water with a pH of 7, suitable for consumption, was employed for both casting and curing. Moreover, the mixture is often formulated and utilized in compliance with ASTM C494 specification type F and is derived from polycarboxylate. Because lightweight aggregate affects workability, LWFRC necessitates the incorporation of a Superplasticizer (SP) to attain an acceptable level of workability.

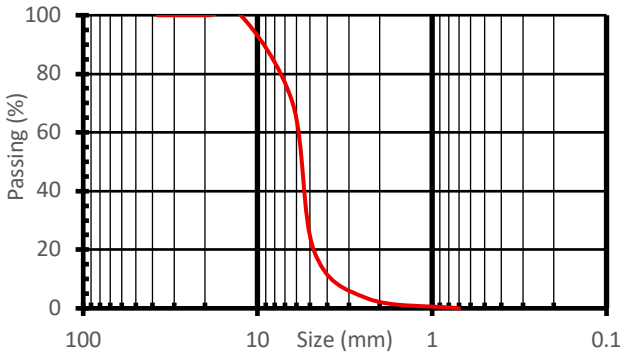

Fig. 1: Grading of crushed limestone used in the LWFRC mixes.

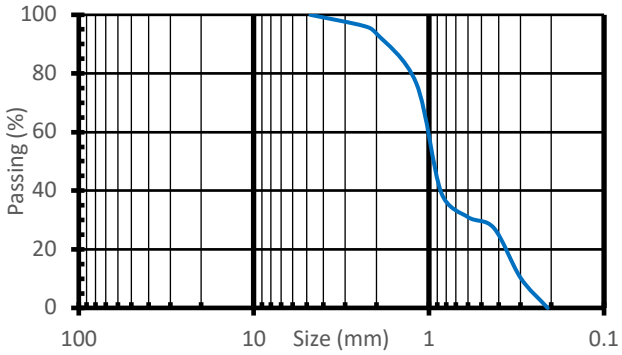

Fig. 2: Grading of sand used in the LWFRC mixes

Class F fly ash according to ASTM 618 was employed for LWFRC, as indicated in Table 3, with 5% retained on a 750 µm sieve and a specific gravity of 2.25. Furthermore, silica fume, including 95.2% SiO2 and adhering to ASTM C1240 standards, was utilized in the formulation of the LWFRC mixes, as detailed in Table 3. In addition, Table 3 presents the chemical composition and physical properties of Ordinary Portland Cement (OPC), fly ash, and silica fume. Using X-Ray Fluorescence (XRF), the chemical compositions of fly ash type F, silica fume, and CEM I 52.5 N were examined.

Expanded perlite (EP) is a naturally occurring amorphous volcanic glass that is generated by increasing its original volume over 35 times through high-temperature heating (700 °C to 1100 °C). The technical and Physical properties of Fine Expanded Perlite are shown in Table 4. Additionally, Fine Expanded Perlite produced by CMB Company is shown in Fig. 3. Expanded Polystyrene Spheres (EPS) were used to produce fibre-reinforced lightweight concrete. The size of the EPS balls used in the FRC Mixture is shown in Fig. 4.

Micro Polypropylene (PP) and Macro End-Hooked Steel (ST) fibers were the two types of fibers used, as illustrated in Fig. 5 and Table 5. Micro (PP) fibers measured 12 mm in length and had an aspect ratio (L_f/d_f) of 400, where L_f and d_f represent the fiber's length and diameter, respectively. PP fibers complied with ASTM C1116 Type III and BS EN 14889-2 standards. However, ST Fibers' aspect ratio (L_f/d_f) of 50 complies with ASTM A820 standards.

Table 3: Chemical compositions and physical properties of CEM I 52.5 N, Fly ash type F, and Silica fume.

Items	**Chemical Composition (%)**		
	CEM I 52.5 N	Fly Ash	Silica Fume
SiO_2	20.80	58.68	95.20
Al_2O_3	4.60	27.70	0.44
Fe_2O_3	2.80	5.41	0.70
CaO	65.40	1.84	1.01
MgO	1.90	0.72	0.10
SO_3	2.20	0.23	-
Na_2O	0.31	0.23	0.10
K_2O	0.44	1.20	< 0.01
TiO_2	-	2.22	0.05
Cl	0.04	0.04	-
Lol	-	0.87	2.19
MnO	-	0.03	0.01
P_2O_5	-	0.58	< 0.01
Cr_2O_3	-	-	-
Free CaO	0.32	-	-
Insoluble residue	1.19	-	-
Hexavalent Chromium	1.91(PPM)	-	-
Specific gravity	3.15	2.32	2.21
Average particle size	1-10 µm	0.19 µm	0.11 µm
Specific surface area (m^2/g)	0.385	10	18
Density	-	0.60 (kg/L)	0.55 (kg/L)

Fig. 3: Fine expanded perlite used in the LWFRC mixes.

Fig. 4: The size of EPS used in the LWFRC mixes.

Table 4: Physical properties of fine expanded perlite used in the LWFRC mixes

Appearance / Color	**Greyish white**
Bulk- Density	142-149 kg/m^3
Moisture	0.1-0.3%

a) End-hook steel fiber

b) Polypropylene fiber

Fig. 5: Fibers used in the LWFRC mixes: a) End-hook steel fiber and b) Polypropylene fiber.

Table 5: Fiber properties used in the LWFRC mixes

Fiber	**Steel**	**polypropylene**
Material	Steel	polypropylene
shape	End-Hook	Straight
Length, l_f (mm)	30	12
Thickness (mm)	0.5	0.03-.032
Cross section	rectangular	rounded
Equivalent diameter, d_f (mm)	0.6	0.03
Density (kg/m^3)	7800	910
Modulus of Elasticity (N/mm^2)	200000	5500-5700
Tensile strength (N/mm^2)	>1000	350

2.2 Variables and Mixture Proportions

To investigate the flexural behavior and mechanical characteristics of LWFRC with different densities, nine mixtures were made. Based on the type-specified target density, all nine mixtures are categorized into three groups. Table 6 lists the compositions for each of these mixes.

Table 6: Mix proportions for LWFRC.

Group	**Mix**		**Mix Proportion (kg / m^3)**														
	Name	**Code**	**Binder**			**Lightweight Aggregate**		**Crushed limestone**	**sand**	**water**	**admixture**	**Fiber**			**W/B***	**PE%**	**EPS%**
			Cement	**Fly ash**	**Silica fume**	**Perlite**	**EPS**					**Weight**	**Vf%**	**Type**			
Group 1	L1	D12C	400	---	---	30	8	200	400	180	12	39.25 + 4.55	1.0	E-H Steel Fiber+Micro PP Fiber	0.45	10	40
	L2	D12F	350	50	---												
	L8	D12S	350	---	50												
Group 2	L5	D15C	400	---	---	60	4	300	500	180	12				0.45	20	20
	L7	D15F	350	50	---												

	L6	D15S	350	---	50												
Group 3	L3	D18C	500	---	---												
	L4	D18F	450	50	---	---	6	400	500	200	12				0.40	---	30
	L9	D18S	450	---	50												

*W/B: The ratio between the weight of water and the total weight of binder.

Group 1: Effect of EPS and Perlite on LWFRC With Density of 1200 kg/m³

This group consists of three mixtures (D12C, D12F, and D12S), which are designed to achieve a target density of 1200 kg/m³. All mixtures of this group contain EPS with a volume content of 40%, perlite with a volume content of 10%, and a hybrid fibre volume content of 1% (0.5% PP + 0.5% ST). The main variables in this group are binder material type and content; for mix D12C, the binder was only cement CEMI 52.5N at 400 kg/m³. For D12F, the binder was cement CEMI 52.5N and fly ash at 350 kg/m³ and 50 kg/m³, respectively. In addition, for D12S, the binder was cement CMI 52.5N and silica fume at 350 kg/m³ and 50 kg/m³, respectively.

Group 2: Effect of EPS and Perlite on LWFRC With Density of 1500 kg/m³

D15C, D15F, and D15S are the three mixtures in this group that are intended to reach the target density of 1500 kg/m³. Twenty per cent EPS, 20 per cent perlite, and 1 per cent hybrid fibre volume (0.5 % PP + 0.5% ST) are present in all of this group's mixtures. The types and contents of the binder materials are the primary variable for this group. For mix D15C, the binder was only cement CMI 52.5N at 400 kg/m³. Cement CMI 52.5N and fly ash, with respective contents of 350 and 50 kg/m³, served as the binder for D15F. Furthermore, silica fume and cement CMI 52.5N, with respective contents of 350 and 50 kg/m³, served as the binder for D15S.

Group 3: Effect of EPS and Perlite on LWFRC With Density of 1800 kg/m³

The three mixtures in this group, D18C, D18F, and D18S, are intended to reach a target density of 1800 kg/m³. Thirty per cent EPS, zero per cent perlite, and 1% hybrid fibre volume are present in all of this group's mixtures (0.5% PP + 0.5% ST). This group's primary variable is the types and contents of the binder materials. For mix D18C, the binder was only cement CEMI 52.5N at 450 kg/m³. Cement CEMI 52.5N and fly ash, with respective contents of 400 and 50 kg/m³, served as the binder for D18F. Furthermore, the binder for D18S consisted of silica fume at 50 kg/m3 and CEMI 52.5N at 400 kg/m³.

2.3 Producing Test Specimens and Formulating Casting Mixtures

Crushed limestone, sand, EPS, perlite, cement, and additional material (fly ash or silica fume, if available) were combined for one minute in order to create all mixes. After that, two minutes were spent mixing in 3/4 of the water. Next, a quarter of the water and the superplasticizer are added to the mixture, and it is stirred for three minutes. Lastly, to guarantee a consistent distribution, fibers were added gradually by hand while mixing. Following that, the specimens were cast in compliance with EN 12390-2 [54]. The samples spent twenty-four hours in a mold. At room temperature, these mixes were allowed to cure for 28 days.

In accordance with ECP203-2025 and EN 12390-3 [54], the compressive strength of each LWFRC combination was measured using six cubes (150×150×150 mm) and six cylinders (diameter × length = 75×150 mm). It should be mentioned that tests were conducted on the cubes and cylinders to ascertain the various correlations between their compressive strengths.

Furthermore, as seen in Fig. 6, three 75×150 mm cylinders were tested to ascertain each LWFRC mixture's tensile splitting strength in accordance with EN 12390-6 [54] and ECP203-2025 [40] requirements.

For each LWFRC mixture, the flexural tensile strength was determined by performing three-point bending tests on three prismatic specimens of Length ×Width ×Height = 550 ×150 ×150 mm in accordance with EN 12390-5 [54] and ECP203-2025 [40]. The distance between supports was 450 mm. Fig. 6 shows the dimensions of the prismatic specimens accepted by EN 12390-5 and ECP203-2025, whereas Fig. 7 shows the mold of the beam before its casting.

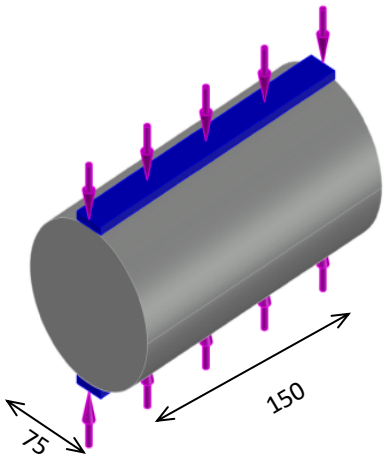

a) Splitting test

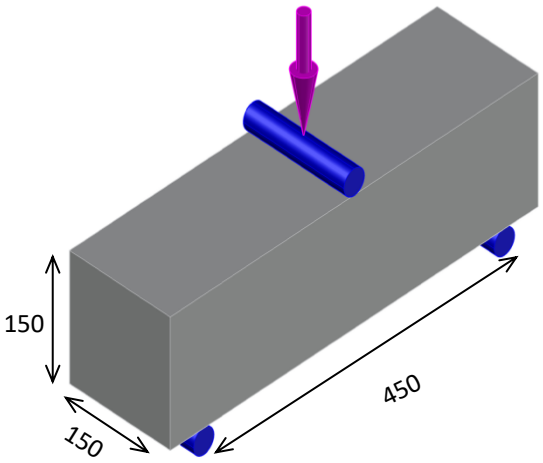

b) Flexure test

Fig. 6: The specimen's necessary dimensions for the following tests: a) splitting test and b) flexure test (measurements in millimeters).

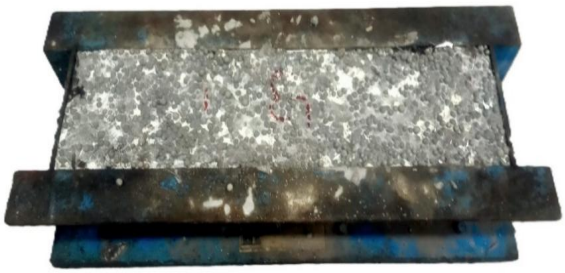

Fig. 7: The beam's mold prior to casting.

2.4 Methods of Testing

According to ACI 544.9R-17 [55], the slump test (ASTM C143/C143M, EN 12350-2, and ECP 203-2025) is commonly used as a straightforward field test to assess the workability of conventional vibrated LWFRC combinations.

ASTM C567, "Standard Test Method for Determining Density of Structural Lightweight Concrete," which addresses both oven-dry and equilibrium density for lightweight structural concrete utilizing lightweight aggregates that satisfy ASTM C330 standards, was followed in determining the density of LWFRC [5]. It should be noted that the specimen used for this test was a cube, not a cylinder. In addition, the density used in this test was the actual density of LWFRC, not the equilibrium density.

In compliance with EN 12390-3, the compressive strength of the previously described cubes and cylinders was assessed by compressive testing after 28 days using a compression testing apparatus with a 2,000 kN capacity. In accordance with EN 12390-6 specification, the cylinders for the splitting tensile test were horizontally loaded in the compression testing apparatus to evaluate the tensile splitting strength after 28 days.

The flexural tensile strength was calculated from a three-point bending test on the beam shown in Fig. 6, in accordance with EN 12390-5. Fig. 8 shows the setup for all these tests.

Additionally, the Schmidt hammer test is used on LWFRC cubes in three distinct orientations (horizontal, downward, and upward) to forecast the compressive strength of LWFRC in a non-destructive manner. To ascertain the tensile splitting strength, the LWFRC cylinders underwent an additional Schmidt hammer test. The Schmidt hammer utilized in this investigation is depicted in Fig. 9. It should be mentioned that specimens were subjected to the Schmidt hammer test prior to the tensile splitting strength and compressive strength tests.

a) Test setup for the slump test

b) Test setup for calculate the density after 28 days

c) Test setup for compression test of the cube

d) Test setup for compression test of the cylinder

e) Test setup for splitting tensile test

f) Test setup for the flexural tensile strength

Fig. 8: Test setup for the tested specimens.

Fig. 9: Schmidt hammer used in this study.

3. Results and Discussions

3.1. Workability

Concrete is divided into five classes (S1, S2, S3, S4, and S5) based on the slump test, per EN 206:2013 [54]. The slump values for each combination are shown in Table 7. Very low workability was indicated by a slump of less than 50 mm for all LWFRC mixtures in all three groups (S1). The slump test results for LWFRC mixture D12F in group 1 are displayed in Fig. 10.

Fig. 10: The slump test for LWFRC mix D12F.

In group 1 of LWFRC mixes with a density of 1200

kg/m3, the slump measurements were 30 mm for mix D12C, 33 mm for mix D12F, and 35 mm for mix D12S. This group exhibits reduced slump values, potentially because of the elevated total volume content of EPS and perlite (50%).

For group 2 of LWFRC mixes with a density of 1500 kg/m3, the slump measurements were 34 mm for mix D15C, 37 mm for mix D15F, and 40 mm for mix D15S. The overall volumetric content of EPS and perlite in the LWFRC mixes within this group was 40%.

For group 3 of LWFRC mixes with a density of 1800 kg/m3, the slump measurements were 39 mm for mix D18C, 42 mm for mix D18F, and 45 mm for mix D18S. This group exhibits elevated slump values, potentially because of the reduced total volume content of EPS and perlite (30%). The water-to-binder ratio in this group is lower than that in the other two groups.

The results show that using EPS and perlite with a total volume content of 30% or more significantly reduces the workability of LWFRC mixes. It may be due to the fact that when EPS and perlite are combined in LWFRC, maintaining workability becomes more challenging due to their combined high absorption (perlite) and low cohesiveness (EPS), exacerbated by the presence of fibers, which further reduces fluidity, especially in the fiber where a hybrid between steel and polypropylene fibers [56, 57].

3.2 Density

Table 7 presents the density values following casting and after 28 days for all LWFRC mixtures. Furthermore, Fig. 11 illustrates the correlation between density post-casting and density after 28 days for all LWFRC mixtures.

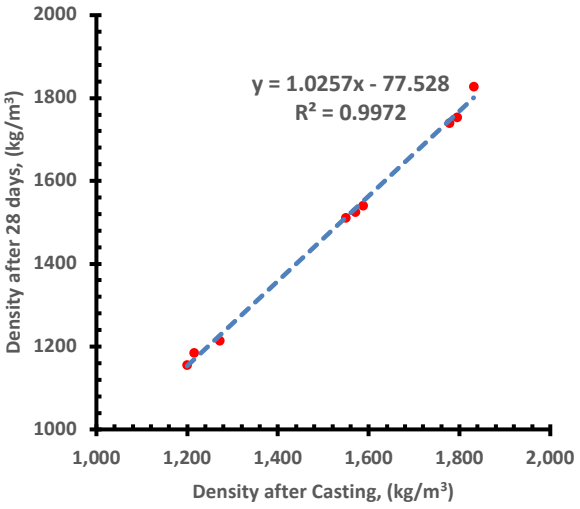

Fig. 11: The relationships between the density after casting and the density after 28 days for all LWFRC mixes.

A summary of the data derived from the graph showing the correlation between post-cast density and post-28-day density for lightweight fibre-reinforced concrete (LWFRC) mixtures is presented below. The scatter plot shows a strong linear relationship between the density immediately after application and that after 28 days. The determination coefficient (R^2) is equal to 0.9972. This almost-perfect correlation shows that the density of fresh concrete in LWFRC mixes containing EPS and perlite is a good predictor of the density of hardened concrete. The regression equation y = 1.0257x-77.528 quantifies this relationship and shows that the density after 28 days can be estimated with a reasonable degree of confidence from the initial density at casting.

After casting, the data points indicate a density range of approximately 1200 kg/m³ to 1800 kg/m³, consistent with the 28-day density range of 1150 kg/m³ to 1800 kg/m³. The closeness of the points along the regression line over the range indicates that the correlation remains constant regardless of the specific concentrations of EPS and perlite in the composition. This consistency is of great benefit to quality control as it shows that variations in the amount of lightweight particles do not change the basic relationship between fresh and hardened density.

The increased R^2 has a significant impact on concrete production and guarantees its quality. Engineers and technicians can accurately predict the LWFRC density after 28 days by assessing the density of freshly mixed concrete immediately after preparation. This means they do not have to wait the full curing time to see if the desired density is achieved. This predictive capability facilitates rapid adjustment of mixture proportions during production and ensures consistency with the design specifications. This relationship indicates that the distribution of lightweight particles remains uniform as the material transitions from fresh to hardened, without segregation or bleeding affecting the final density.

The slight increase in density (approximately 25-50 kg per m³, dependent on the mixture) is negligible in comparison to the overall density values, suggesting that the volumetric changes after dilution are minimal. This stability means that EPS beads and perlite particles remain fixed in the cement matrix during curing, and that the hydration process compensates for any small size variations. The absence of significant density loss indicates that the lightweight aggregates do not absorb excess water and do not degrade during curing. It is crucial to sustain the structural integrity and consistent performance of the LWF components.

3.3 Compressive strength

The compressive strength outcomes for each LWFRC mixture are shown in Table 7. After 28 days, the cube compressive strengths for each specimen using a cube size of 150×150×150 mm and a cylinder size of 75×150 mm are displayed in Fig. 12. The figure compares the cylinder

strength (f_c') and cube strength (f_{cu}) values for nine distinct LWFRC specimens using compressive strength data, which is shown as a radar chart (a) and a bar chart (b).

Table 7: Results for all LWFRC mixtures, including workability, density, compressive strength, tensile splitting strength, and modulus of rupture.

Group		Group 1			Group 2			Group 3		
Mix		D12C	D12F	D12S	D15C	D15F	D15S	D18C	D18F	D18S
Workability	Slump (mm)	30	33	35	34	37	40	39	42	45
Density (kg/m^3)	γ casting	1271.11	1214.81	1200.00	1588.15	1570.37	1549.63	1831.11	1795.56	1777.78
	γ 28 days	1214.81	1185.19	1155.56	1540.74	1525.93	1511.11	1828.15	1754.07	1739.26
Compressive strength (N/mm^2)	f_{cu}	5.04	5.18	5.34	11.42	12.00	12.66	25.80	25.89	26.21
	f_c'	4.49	4.51	4.59	10.39	10.68	10.89	22.70	22.78	22.81
	f_c'/f_{cu}	0.89	0.87	0.86	0.91	0.89	0.86	0.88	0.88	0.87
Tensile splitting strength (N/mm^2)	f_{sp}	1.10	1.18	1.27	2.65	2.66	2.75	4.37	4.47	4.67
	$f_{sp}/\sqrt{f_{cu}}$	0.49	0.52	0.55	0.78	0.77	0.77	0.86	0.88	0.91
Modulus of rupture (N/mm^2)	f_{ctr}	1.55	1.65	1.70	3.00	3.20	3.40	5.00	5.10	5.30
	$f_{ctr}/\sqrt{f_{cu}}$	0.69	0.72	0.74	0.89	0.92	0.96	0.98	1.00	1.04
f_{sp}/f_{ctr}		0.71	0.72	0.75	0.88	0.83	0.81	0.87	0.88	0.88

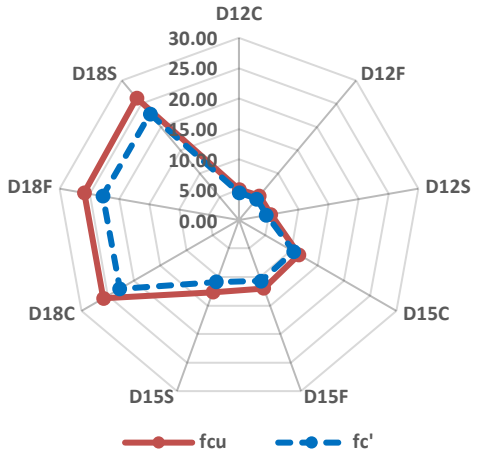

a)

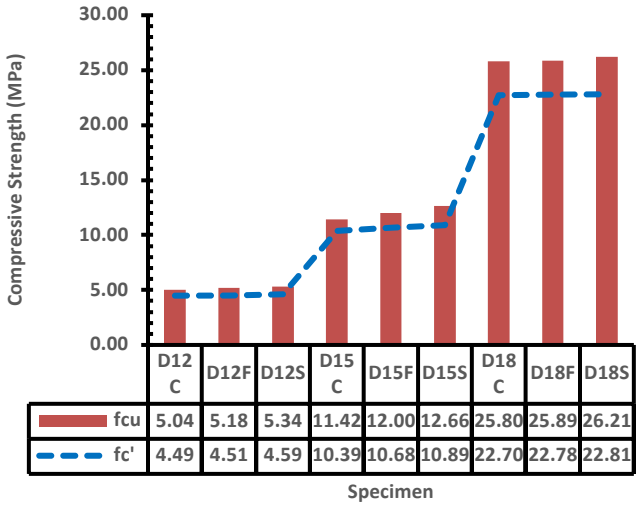

b)

Fig. 12: The compressive strength cylinders and cubes for the LWFRC mixes in this study.

The experimental results reveal significant differences in the compressive strength of the different compositions. Samples can be classified into three different performance groups:

- Group 1 (D12C, D12F, D12S), with EPS and perlite volume content of 50%, was classified as the low-strength group; these samples had compressive strengths between 5.04 and 5.34 MPa, representing the minimum performance with minimal fibre or light aggregate incorporation. The strengths of cylinders and cubes show minimal variation, indicating consistent material behaviour at lower levels of strength. Also, it should be noted that the specimens with 50 kg/m^3 of cement replaced by supplementary materials show improved compressive strength, especially the specimen with silica fume D12S.
- Group 2 (D15C, D15F, D15S), with EPS and perlite volume content of 40%, classified as the medium-strength group, demonstrated enhanced performance, exhibiting a compression factor of 11.42-12.66 MPa, about 100% greater than that of the low-strength group. This notable enhancement delivers an ideal fibre-to-aggregate ratio, enhancing the concrete matrix while preserving its density. Furthermore, it is noteworthy that specimens with 50 kg/m3 of cement replaced by supplementary materials exhibit enhanced compressive strength, particularly those containing silica fume D15S.
- Group 3 (D18C, D18F, D18S), without perlite and with an EPS volume content of 30%, comprised the high-strength samples, achieving compressive strengths of 25.80-26.21 MPa, demonstrating the successful optimization of the lightweight fibre-reinforced concrete mixture design. The results indicate that lightweight concrete can attain the strength levels of structural-grade concrete. Furthermore, it is important to note that specimens with 50 kg/m3 of cement replaced by supplementary materials exhibit enhanced compressive

strength, particularly the specimen containing silica fume D18S.

The relationship between the cylinder (f_c') and cube (f_{cu}) strengths follows the expected trend, with cube strengths consistently higher than cylinder strengths across all samples. The strength ratio (f_c'/f_{cu}) remains relatively constant at about 0.85-0.90, which is in line with the conversion factors that have been set. It should be noted that this ratio is nearly identical to the ratio proposed by ECP 203-2025 for normal-weight concrete.

Fig. 13 illustrates the correlation between cube compressive strength and density after 28 days for the lightweight fiber-reinforced concrete (LWFRC) mixtures examined in this study. The graphic illustrates a robust, nonlinear association between 28-day cube density and compressive strength. The graphic indicates that the compressive strength of LWFRC may be predicted as a function of its density, utilizing a hybrid fiber content of 1%, through a second-order polynomial relationship as follows:

$$f_{cu} = 5 \times 10^{-5}\,\gamma^2 - 0.1077\,\gamma + 65.31 \qquad \text{(Eq. 1)}$$

with $R^2 = 0.961$.

Where:

f_{cu} is the LWFRC compressive strength of a cube 150×150×150 mm (N/mm^2), and γ is the density of LWFRC after 28 days(kg/m^3).

The findings demonstrated that as the hardened density of lightweight fiber-reinforced concrete (LWFRC) escalates from roughly 1200 kg/m³ to 1800 kg/m³, the cube compressive strength increases significantly:

- Low density (≈1200 kg/m³): Strength ≈ 5 MPa
- Medium density (≈1500 kg/m³): Strength ≈ 12 MPa
- High density (≈1800 kg/m³): Strength ≈ 27 MPa

This suggests that a small increase in density produces a disproportionate increase in force once the threshold value (about 1500 kg/m³) is reached.

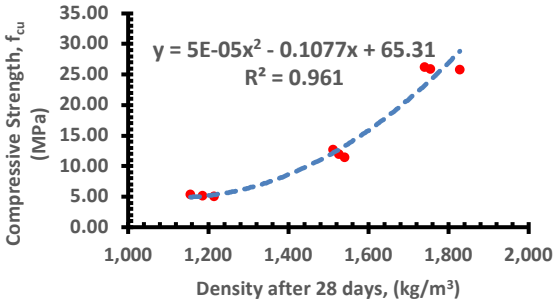

Fig. 13: The relationship between the cube compressive strength and density after 28 days for LWFRC mixes in this study.

Fig. 14 illustrates the fracture formation for the cubes and cylinders of all compositions. The results demonstrate that decreasing the volume proportion of EPS and perlite from 50% to 30% increased the density from 1200 to 1800 kg/m^3, resulting in a substantial increase in concrete compressive strength from around 5 MPa to approximately 27 MPa. Moreover, it is crucial to note that all LWFRC specimens in this investigation, with 50 kg/m^3 of cement replaced by supplementary materials, demonstrate improved compressive strength, especially those with silica fume (D12S, D15S, and D18S).

Fig. 14: The fracture formation for all LWFRC mixtures, cubes, cylinders, and splitting in cylinders.

3.4 Tensile splitting strength

The fracture pattern of the cylinders splitting for each LWFRC mixture is displayed in Fig. 14. The tensile splitting strengths of 75×150 cylinders for all mixes after 28 days are displayed in Fig. 15 and Table 7. Generally, the tensile splitting strength for all mixtures shows the same trend as the cube compressive strength. The dual presentation format—radar chart (a) and bar chart (b)—offers complementary perspectives on the data. The radar chart effectively illustrates the relative performance of all mixes simultaneously, making it easy to visualize the hierarchy of tensile strength across specimens. The nearly circular shape, with pronounced expansion toward the D18 series specimens, clearly shows the superior performance of high-density, fibre-rich mixes. The bar chart provides a more precise quantitative comparison, allowing for exact value determination and direct

magnitude comparisons between adjacent mix designs. Both representations confirm the step-wise improvement pattern across the three density levels.

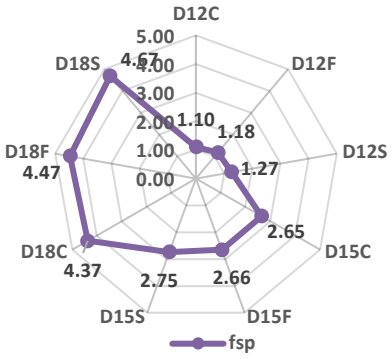

a)

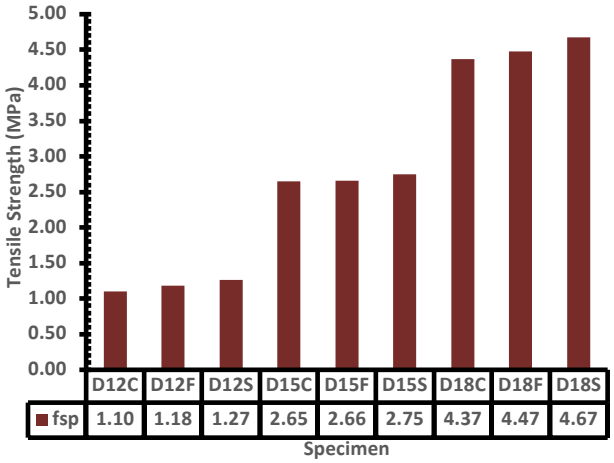

b)

Fig. 15: The tensile splitting strength of all LWFRC mixes.

The tensile splitting strength shows a distinct, systematic increase as the content of EPS and perlite decreases across the mix designs. Specimens from group 1 (D12C, D12F, D12S) demonstrate the lowest splitting tensile strengths, varying from 1.10 to 1.27 MPa, indicating the baseline performance of LWFRC with 50% volume content of EPS and perlite. As the volume content of EPS and perlite diminishes from medium-density specimens (D15C, D15F, D15S at 2.65-2.75 MPa) to high-density specimens (D18C, D18F, D18S at 4.37-4.67 MPa), the tensile splitting strength escalates by about 325% from the lowest to the highest performing mixtures. This significant enhancement highlights the essential role of EPS and perlite volume content in enhancing the tensile strength of LWFRC.

The specimen identification pattern indicates that the supplemental material, when substituted with cement (denoted by the prefixes C, F, and S), yields generally uniform results within each density category, with differences of less than 10% among specimens of comparable density levels. The D18S specimen attained the maximum tensile splitting strength of 4.67 MPa, closely followed by D18F at 4.47 MPa and D18C at 4.37 MPa, demonstrating that all three supplemental materials, when substituted for cement at the highest density level, exhibit remarkable performance. The intermediate group (D15 series) is quite consistent, with values ranging from 2.65 to 2.75 MPa. This means that the behavior at this compositional level is stable and predictable. The fact that the density groups are identical shows that the quality control, mixing, and testing methods can be repeated.

Fig. 16 shows the relationship between the tensile splitting strength (f_{sp}) of all 75×150 mm LWFRC cylinders and the density after 28 days. The results reveal a strong correlation between concrete density (as indicated by the specimen designation) and tensile splitting strength. The D12 series (lowest density, with higher EPS and perlite content) exhibits the lowest tensile strengths due to reduced cement paste volume and the presence of more weak interfacial transition zones around lightweight aggregate particles. The D15 series shows approximately double the tensile strength, while the D18 series (highest density, lower lightweight aggregate content) achieves nearly quadruple the strength of the D12 series. This trend indicates that while lightweight aggregates successfully reduce density, they also create discontinuities in the stress transfer mechanism during tensile loading. The fibre reinforcement partially compensates for this effect, but the fundamental roles of paste density and aggregate volume fraction remain dominant in determining splitting tensile capacity.

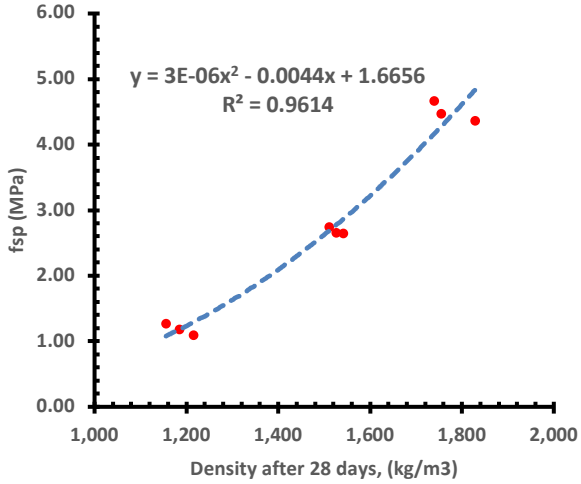

Fig. 16: The relationship between f_{sp} and density after 28 days for LWFRC mixes in this study.

A significant, nonlinear escalation in splitting tensile strength (f_{sp}) occurs with the augmentation of hardened concrete density, demonstrating that denser LWFRC mixtures demonstrate disproportionately enhanced tensile capacity. The data are accurately represented by a

second-order polynomial regression as follows:

$$f_{sp} = 3 \times 10^{-6}\,\gamma^2 - 0.0044\,\gamma + 1.6656 \quad \text{(Eq. 2)}$$

Where:

f_{sp} is the LWFRC splitting tensile strength of a cylinder 75×150 mm (N/mm^2), and γ is the density of LWFRC after 28 days (kg/m^3).

With a coefficient of determination R^2=0.9614. This high R^2 indicates that the second-order polynomial model accounts for over 96% of the variability in tensile strength across the tested density range. Fig.17 illustrates the correlation between the ratio $f_{sp}/\sqrt{f_{cu}}$ and the density after 28 days for all LWFRC mixtures. The ratio $f_{sp}/\sqrt{f_{cu}}$ was about 0.55 for LWFRC mixes with a density of 1200 kg/m^3, about 0.77 for LWFRC mixes with a density of 1500 kg/m3, and 0.90 for LWFRC mixes with a density of 1800 kg/m^3. It should be noted that the value of the ratio $f_{sp}/\sqrt{f_{cu}}$ for LWFRC exceeds the value (0.42) recommended by ECP203-2025 for normal weight concrete. The crack-bridging mechanism of fiber reinforcement is responsible for the significant increase in splitting tensile strength with increasing density in LWFRC. A vertical fracture plane is produced in the splitting tensile test when the specimen is subjected to tensile stresses perpendicular to the loading direction. The concrete matrix contains fibres that block potential fracture paths, preventing cracks from initiating and spreading. Greater tensile load-carrying capacity is the result of a proportional increase in the number of fibers crossing any potential crack plane as fiber content rises. The roughly fourfold improvement from D12C to D18S shows that a sufficient dosage of fiber produces a more ductile reaction instead of the brittle tensile behavior that characterizes plain concrete. The figure clearly shows that tensile splitting strength is proportional to the square root of the compressive strength, and once the compressive strength is obtained, the tensile splitting strength can be expected as a ratio of ($\sqrt{f_{cu}}$) with respect to the LWFRC density.

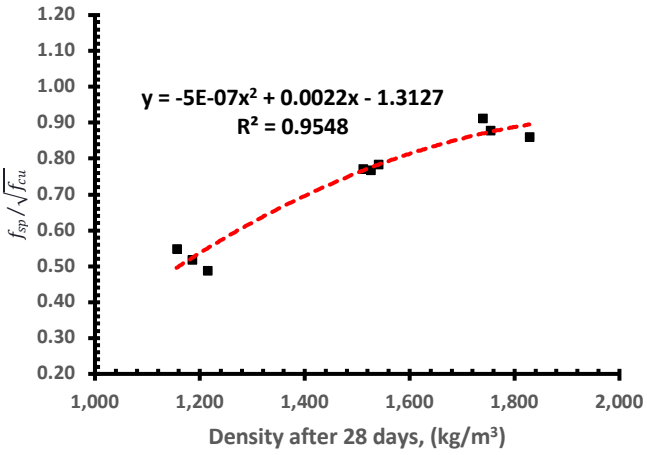

Fig. 17: Ratio of $f_{sp}/\sqrt{f_{cu}}$ Versus the density after 28 days for LWFRC mixes in this study.

There is a strong, nonlinear increase in the ratio $f_{sp}/\sqrt{f_{cu}}$ with increasing hardened concrete density, indicating that denser LWFRC mixes exhibit a disproportionately higher ratio $f_{sp}/\sqrt{f_{cu}}$. The data are well described by a second-order polynomial regression as follows:

$$f_{sp}/\sqrt{f_{cu}} = -5 \times 10^{-7}\,\gamma^2 + 0.0022\,\gamma - 1.3127 \quad \text{(Eq. 3)}$$

Where:

f_{cu} is the LWFRC compressive strength of a cube 150×150×150 mm (N/mm^2), f_{sp} is the LWFRC splitting tensile strength of a cylinder 75×150 mm (N/mm^2), and γ is the density of LWFRC after 28 days (kg/m^3).

With a coefficient of determination R^2=0.9548. This high coefficient of determination indicates that over 95% of the variability in normalized tensile capacity is explained by density alone.

3.5 The Flexural behavior

This section analyzes the flexural behaviour of each specimen by assessing the flexural tensile strength (f_{ctr}) and the modulus of rupture. The modulus of rupture (f_{ctr}) represents the maximum flexural tensile strength that a beam section can withstand, determined by Equation 4.

$$f_{ctr} = \frac{3F_{max}L}{2bh^2} \quad \text{(Eq. 4)}$$

Where:

F_{max} denotes the maximum applied flexural load (N), L represents the span of the beam (mm), b indicates the width of the beam (mm), and h signifies the height of the beam (mm).

Fig. 18 illustrates the fracture forms of the tested beams subjected to flexural test for the LWFRC mixture D15F in this investigation. Table 3 and Fig. 19 display the flexural tensile strength results for the two groups. Fig. 19 presents two charts: first, the radar chart highlights the relative performance hierarchy among all nine mixes, clearly showing the outward expansion for the D18 series. While the second, a bar-and-line chart, presents exact splitting strength values (solid bars) alongside flexural strength data as a dashed trendline, emphasizing the nonlinear increase in strength with density.

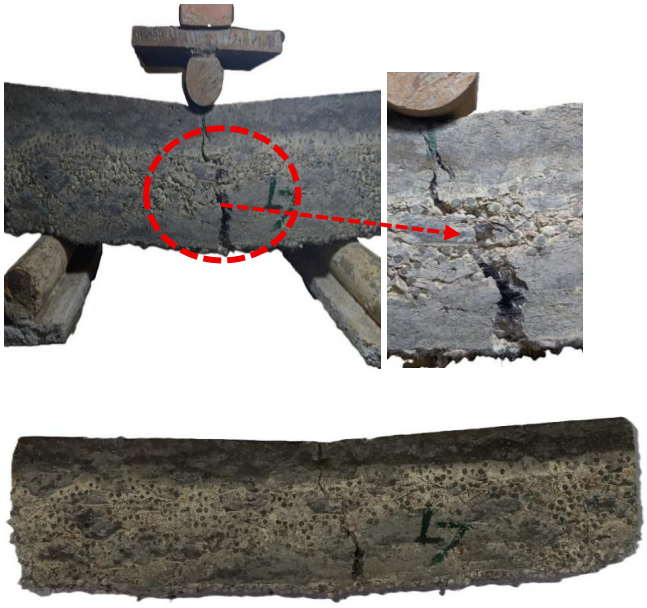

Fig. 18: The crack patterns of the tested beam D15F under flexure.

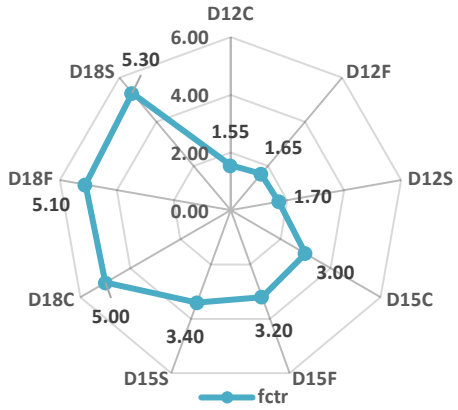

a)

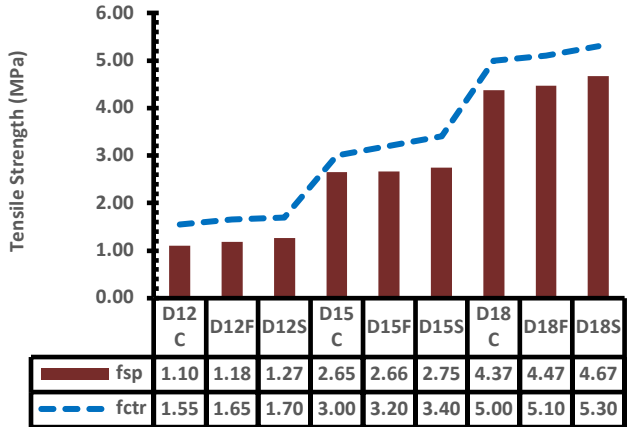

b)

Fig. 19: The flexural tensile strength of all LWFRC mixes.

The flexural tensile strength exhibits an apparent, systematic increase as the proportions of EPS and perlite diminish in the mix designs. Specimens from group 1 (D12C, D12F, D12S) exhibit the lowest flexural tensile strengths, ranging from 1.55 to 1.70 MPa, signifying the baseline performance of LWFRC with 50% volume content of EPS and perlite. As the volumetric proportions of EPS and perlite decrease from medium-density specimens (D15C, D15F, D15S at 3.00-3.40 MPa) to high-density specimens (D18C, D18F, D18S at 5.00-5.30 MPa), the flexural tensile strength increases by approximately 325% from the lowest to the highest performing combinations. This notable improvement underscores the critical importance of EPS and perlite volume content in augmenting the tensile strength of lightweight fibre-reinforced concrete. Under bending, tensile stresses concentrate at the tension face, causing cracks that initiate at the bottom surface. Fibers intersect these cracks and transfer load across the opening through pull-out and debonding mechanisms. As density increases, 1) The matrix confinement enhances fiber anchorage. 2) Interfacial transition zones around lightweight aggregates become less prevalent, reducing weak points. 3) The cumulative effect is a higher flexural capacity per unit fiber content.

In general, the tensile splitting strength and the flexural tensile strength for all mixtures exhibit nearly identical trends. The ratio f_{sp} / f_{ctr} is about 0.73 for LWFRC mixes with a density of 1200 kg/m^3, about 0.84 for LWFRC mixes with a density of 1500 kg/m^3, and 0.88 for LWFRC mixes with a density of 1800 kg/m^3. Notably, the ratio of f_{sp} / f_{ctr} for LWFRC is greater than the 0.70 value suggested by ECP203-2025 for normal-weight concrete.

Fig. 20 shows the relationship between the concrete flexural tensile strength (f_{ctr}) and the density after 28 days for all LWFRC mixtures. The results reveal a strong correlation between concrete density (as indicated by the specimen designation) and flexural tensile strength. The D12 series (lowest density, with higher EPS and perlite content) exhibits the lowest tensile strengths due to reduced cement paste volume and the presence of more weak interfacial transition zones around lightweight aggregate particles. The D15 series shows approximately double the tensile strength, while the D18 series (highest density, lower lightweight aggregate content) achieves nearly quadruple the strength of the D12 series. This trend indicates that while lightweight aggregates successfully reduce density, they also create discontinuities in the stress transfer mechanism during tensile loading. The fibre reinforcement partially compensates for this effect, but the fundamental roles of paste density and aggregate volume fraction remain dominant in determining splitting tensile capacity.

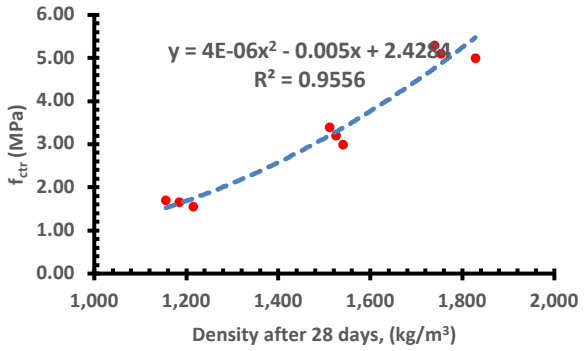

Fig. 20: The relationship between f_{ctr} and density after 28 days for LWFRC mixes in this study.

There is a strong, nonlinear increase in flexural tensile strength (f_{sp}) with increasing hardened concrete density, indicating that denser LWFRC mixes exhibit disproportionately higher tensile capacity. The data are well described by a second-order polynomial regression as follows:

$$f_{ctr} = 4 \times 10^{-6}\,\gamma^2 - 0.005\,\gamma + 2.4284 \qquad \text{(Eq. 5)}$$

Where:

f_{ctr} is the LWFRC flexural tensile strength (N/mm^2), and γ is the density of LWFRC after 28 days (kg/m^3).

With a coefficient of determination R^2=0.9556. This high R^2 indicates that the second-order polynomial model accounts for over 95% of the variability in flexural tensile strength across the tested density range. Fig.21 illustrates the correlation between $f_{ctr}/\sqrt{f_{cu}}$ and the density after 28 days for all LWFRC mixtures. The ratio $f_{ctr}/\sqrt{f_{cu}}$ about 0.72 for LWFRC mixes with a density of 1200 kg/m^3, about 0.92 for LWFRC mixes with a density of 1500 kg/m^3, and 1.00 for LWFRC mixes with a density of 1800 kg/m^3. It should be noted that the value of the ratio $f_{ctr}/\sqrt{f_{cu}}$, for all LWFRC with varied densities, exceeds the value (0.60) predicted by ECP203-2025 for normal-weight concrete.

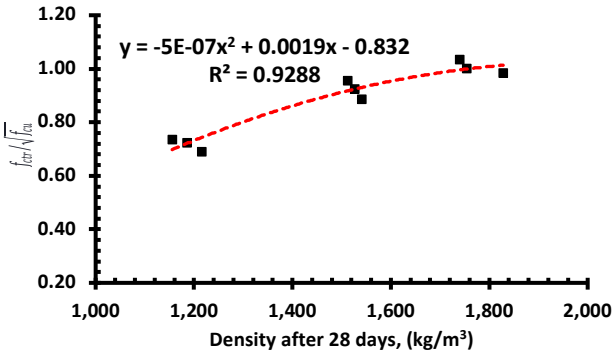

Fig. 21: Ratio $f_{ctr}/\sqrt{f_{cu}}$ versus the density after 28 days for LWFRC mixes in this study.

There is a substantial, nonlinear increase in the ratio $f_{ctr}/\sqrt{f_{cu}}$ with increasing hardened concrete density, indicating that denser LWFRC mixes exhibit a disproportionately higher ratio $f_{ctr}/\sqrt{f_{cu}}$. The data are well described by a second-order polynomial regression as follows:

$$f_{ctr}/\sqrt{f_{cu}} = -5 \times 10^{-7}\,\gamma^2 + 0.0019\,\gamma - 0.832 \qquad \text{(Eq. 6)}$$

Where:

f_{cu} is the LWFRC compressive strength of a cube 150×150×150 mm (N/mm^2), f_{ctr} is the LWFRC flexural tensile strength (N/mm^2), and γ is the density of LWFRC after 28 days (kg/m^3).

With a coefficient of determination R^2=0.9288. This high coefficient of determination indicates that over 92% of the variability in normalized flexural tensile capacity is explained by density alone. The findings demonstrate that the normalized flexural tensile efficiency of LWFRC increases with density but exhibits declining returns at higher densities, suggesting an optimal density range for effective fibre reinforcement in bending applications.

3.6 Shemidit hammer

For non-destructive surface hardness testing and compressive strength estimation of lightweight fiber-reinforced concrete (LWFRC) containing hybrid fibers, the Schmidt hammer is appropriate [58, 59]. Compared with conventional lightweight mixes, research indicates that adding hybrid fibers (such as steel, glass, polypropylene, or mixtures) to lightweight concrete often results in a higher Schmidt rebound number, particularly after 28 days, which is directly correlated with improved compressive strength [60, 61].

Adding fiber to lightweight concrete raises rebound values more than adding it to regular-weight concrete. It also makes the surface harder and stronger when using the Schmidt hammer. [60, 61]. The rebound number from Schmidt hammer testing may not give an accurate picture of real compressive strength when compared to direct compression tests. However, it does give an accurate picture of how hybrid fibers affect surface and compressive strength [62, 63]. The substantial correlation between mechanical strength and rebound number validates the benefits of hybrid fiber-reinforced mixes; an elevated fiber content, especially in lightweight concrete, enhances both compressive strength and rebound value [60, 64].

The relationship between rebound values and compressive strength is influenced by aggregate type, fiber content, and density; therefore, results for LWFRC with hybrid fibers must be evaluated using calibration curves created for analogous combinations [60, 65].

3.6.1 Compressive Strength

The Schmidt hammer test was performed on all LWFRC cube specimens in three positions to calibrate the used shmedit hammer and obtain the compressive strength of LWFRC with hybrid fibres. Fig. 22 shows the three positions (downward, horizontal, and upward) performed during the Schmidt hammer test.

a) downward

b) horizontal

c) upward

Fig. 22: The three positions performed during the Schmidt hammer test used in this study: a) downward, b) horizontal, and c) upward.

Fig. 23 shows the relationship between f_{cu} and the rebound number for normal-weight concrete proposed by the Schmidt hammer used in this study. It is necessary to use bespoke calibration rather than general manufacturer curves because the type of aggregate, fibre content, and concrete density can all vary. The next calibration method used was as follows:

1. At least six representative samples of the lightweight hybrid fiber composite must be manufactured, properly cured, and tested at appropriate ages.
2. When the surface of each specimen is ready (it should be smooth, dry, and free of dust), measure the rebound number on a grid across its three faces and positions.
3. Follow ASTM C39, EN 12390-3, or ECP 203-2025 standards to test the compressive strength of the same samples.
4. Use a statistical model, like linear regression, to graph the relationship between the recorded compressive strengths and rebound values. R^2 values not less than 0.92 are best.
5. Use this curve to interpret results from in situ or similar lightweight hybrid-fiber concrete samples.

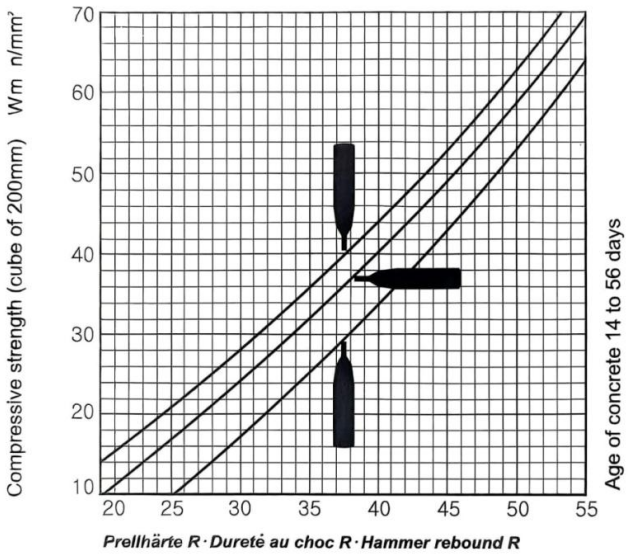

Fig. 23: The relationship between f_{cu} and the rebound number for normal-weight concrete proposed by the Schmidt hammer used in this study.

Fig. 24 shows how fcu and rebound number are related for each cube at the three directions for LWFRC mixes in this investigation. Lightweight fibre-reinforced concrete (LWFRRC) combinations exhibit rebound-strength relationships different from those of regular normal-weight concrete. This is shown by the rebound hammer results in Figs. 23 and 24. The direction of the measurement affects the estimated compressive strength.

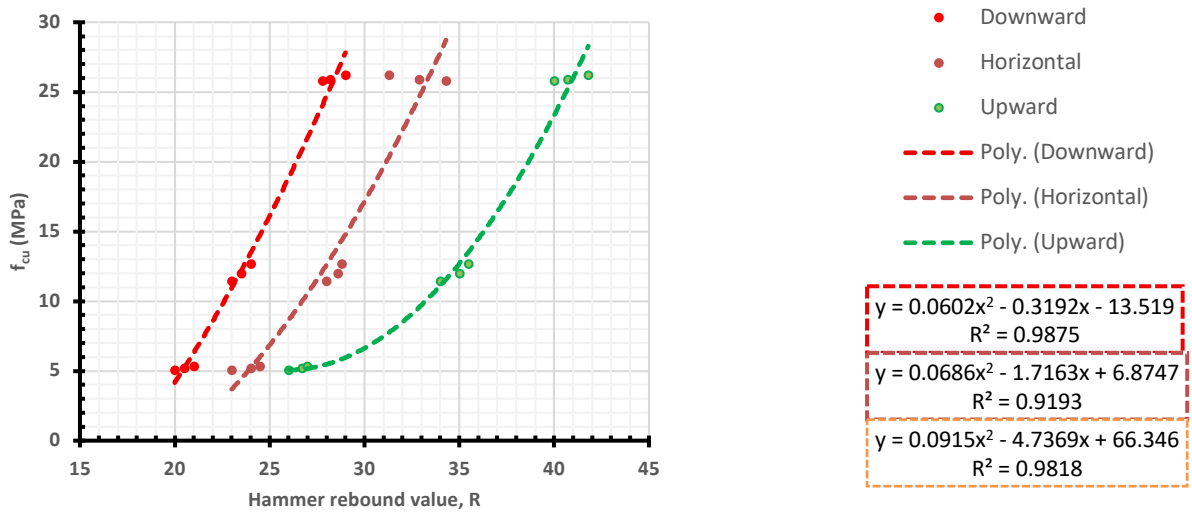

Fig. 24: The relationship between f_{cu} and the rebound number for LWFRC mixes in this study.

The regular Schmidt-hammer curve (Fig. 23) and the polynomial approximations for the LWFRRC mixes (Fig. 24) are very different from each other. All three orientations in Fig. 24 have higher rebound values for a given compressive strength than the normal-weight concrete curve. This change shows that adding lightweight fibers and aggregates makes the surface harder without making the cube stronger, which means that normal calibration curves are not safe for LWFRRC.

The second-order polynomial regression that follows is based on three measurement directions: downward (effect on a downward-facing surface), horizontal (effect on a vertical surface), and upward (effect on the underside), as follows:

Downward:

$$f_{cu} = 0.0602R^2 - 0.3192R - 13.519 \quad \text{(Eq. 7)}$$

(with a coefficient of correlation $R^2 = 0.9875$)

Horizontal:

$$f_{cu} = 0.0686R^2 - 1.7163R + 6.8747 \quad \text{(Eq. 8)}$$

(with a coefficient of correlation $R^2 = 0.9193$)

Upward:

$$f_{cu} = 0.0915R^2 - 4.7369R + 66.346 \quad \text{(Eq. 9)}$$

(with a coefficient of correlation $R^2 = 0.9818$)

In the underlying measurement, where fiber distribution and aggregate orientation are expected to affect local stiffness, the upward orientation shows the biggest intercept and the steepest quadratic coefficient. This means that the rebound sensitivity is higher.

Second-order polynomials accurately show the connection between rebound and strength across orientations. This is shown by the high coefficients of determination (R^2 > 0.92) achieved in all regression analyses for LWFRRC mixes. The horizontal orientation has the lowest R^2 (0.9193), which means there is a little more spread. This could be because the surface finishing of vertical surfaces isn't always the same.

The study emphasizes the imperative to create rebound calibration curves for LWFRRC tailored to distinct mixtures and orientations. When using standard Schmidt-hammer correlations, the in-situ compressive strength may be very wrong. Using the suggested polynomial relationships will improve the accuracy of the non-destructive strength test for lightweight fibre-reinforced concrete.

3.6.2 Tensile splitting strength

This part describes a Schmidt hammer test performed in the downward direction on LWFRC cylinders to calibrate a curve and obtain the splitting tensile strength of LWFRC with varied densities without destructive testing, as shown in Fig. 25. Fig. 26 shows the results and the relationship between f_{sp} of a 75×150 mm cylinder and the rebound number for LWFRC mixes in this study.

Fig. 25: The pSchmidt hammer test performed in the downward direction on LWFRC cylinders.

Fig. 26 presents the correlation between the hammer rebound value (R) and splitting tensile strength (f_{sp}) for lightweight fiber-reinforced concrete (LWFRRC) mixes, captured by the polynomial equation:

$$f_{sp} = 0.0022R^2 + 0.1905R - 3.991 \quad \text{(Eq. 10)}$$

with an impressive coefficient of determination, R^2 = 0.9966.

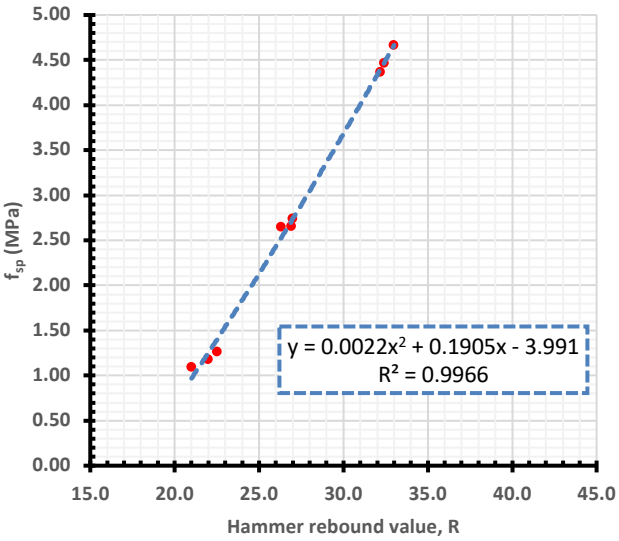

Fig. 26: The relationship between f_{sp} and the rebound number for LWFRC mixes in this study.

The best 2nd-order polynomial trend shows that the f_{sp} value rises faster as the rebound index increases, especially when the R value is above about 30. At higher mix strengths, the combined effect of lightweight particles and fibres may be seen in the increasing surface hardness and the strengthening of the internal matrix, as shown by this non-linear trend. The need for mix-specific curves is validated by the unique polynomial calibration for splitting tensile strength, which differs from the correlations for compressive strength shown in Figs. 23 and 24. General calibrations for normal-weight concrete do not apply to LWFRRC because its matrix behaves in an atypical manner.

Using a rebound hammer makes it easy and quick to measure the splitting tensile strength of fiber-reinforced lightweight concrete. This speeds up structural examinations and reduces the need for risky samples. Because the curve and the real data are so closely related, more research is needed to confirm this link across different mix changes (types of fiber, doses, aggregate gradations) and environmental factors. Nonetheless, the current equation offers a solid basis for the LWFRRC combinations examined in this study.

The findings demonstrate that the calibrated rebound hammer test is a viable method for assessing the splitting tensile strength of LWFRRC. To determine the efficacy of similar combinations in situ, the formula derived from the study must be utilized. This would enable examination of the structure and quality of lightweight, fibre-reinforced concrete.

4. Numerical Modeling of LWFRC Beams

This part delineates the numerical analysis model for the examined LWFRC beams utilizing the Finite Element Modelling (FEM) software ANSYS Workbench 2023 R2 [53]. The data encompasses discretized geometry, element section attributes, material specifications, analysis type, and output results. The specifications of the tested LWFRC beams are shown in Fig. 6. [18, 66]. Furthermore, Table 6 provides information on groups 1, 2, and 3 of the LWFRC-tested beams.

4.1 Distinct Element Types and Geometry

The three-dimensional eight-node element CPT215 was used to simulate the concrete beam. Beams spanning 150 × 150 × 550 mm were split into 12.5 × 12.5 × 12.5 mm pieces for analysis. Fig. 27 shows the concrete beam meshing with the 8-node brick element CPT215. In contrast, the 50 x 150 mm steel loading cylinder and supports were split into 12.5 x 12.5 x 12.5 mm sections. Fig. 27 shows the 8-node brick element SOLID185 representing the steel loading cylinder and supports.

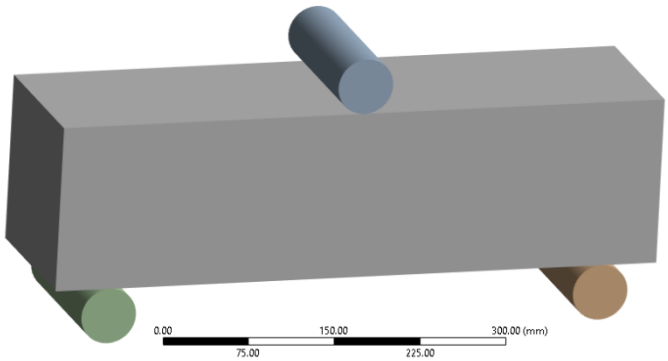

a) Geometry

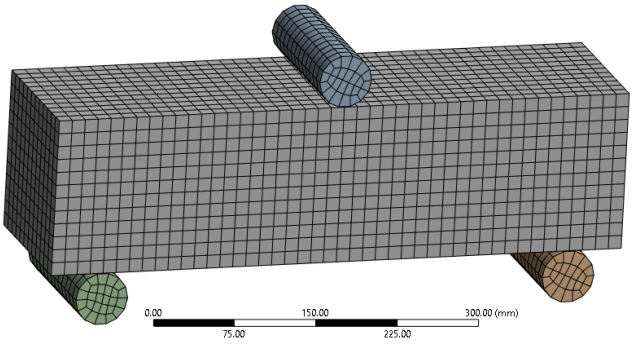

b) Meshing

Fig. 27: Modelling of LWFRC beams.

4.2 Materials

For concrete, a coupled damage-plasticity microplane model is used in CPT215, one of the concrete elements in ANSYS. The study of Bazant and Gambarova, which predicts material behavior across a range of individual planes using stress-strain laws, served as the foundation for the microplane model. By applying damage rules to specific potential failure planes, directional-dependent stiffness deterioration is simulated, yielding a macroscopic anisotropic damage formulation. The model use 42 microplanes for numerical integration. Since twenty-one microplanes are symmetrical—that is, each plane has the same normal direction—they are considered [53, 67, 68]. The model's implicit gradient regularisation introduces two additional degrees of freedom per node, implemented via a nonlocal field. The components of total strain are decomposed additively into elastic and plastic components [69-72]. To simulate concrete material in ANSYS utilizing a linked damage-plasticity microplane model, four parameter types—elasticity, plasticity, damage, and nonlocal—must be established, as illustrated in Table 8 [2].

Table 8: Parameters for defining Material.

Parameter Type	**Parameter Subtype**	**Parameter**	**The proposed value for LWFRC beams**
Material parameters for the concrete using the coupled damage-plasticity microplane model			
Elasticity	-----	Modulus of elasticity, E_c (N/mm^2)	According to experimental results
	-----	Poisson's ratio, u_c	0.2
Plasticity	Drucker-Prager yield function	Uniaxial compressive strength, f_c' (N/mm^2)	According to experimental results
		Biaxial compressive strength, f_{bc} (N/mm^2)	$1.15\,f_c'$
		Uniaxial tensile strength, f_t (N/mm^2)	According to experimental results
	Compression cap	Intersection point abscissa between compression cap and Drucker-Prager yield function, σ_v^c	$\sigma_v^c = -\frac{2}{3} f_{bc}$
		The ratio between the major and minor axes of the cap, R	2.0
	Hardening	Hardening material constant, D	40000
		Tension cap hardening constant, R_T	1.0
Damage	-----	Tension damage thresholds, γ_{t0}	0.0
	-----	Compression damage thresholds, γ_{c0}	2e-6
	-----	Tension damage evolution constants, β_t	0.4e4
	-----	Compression damage evolution constants, β_c	0.25e4
Nonlocal	-----	Nonlocal interaction range parameter, c	156.25 (related to the length scale parameter (l) by the equation $c=l^2$)
	-----	Over-nonlocal averaging parameter, m	2.5
Material parameters for steel loading cylinder and steel supports			
Elasticity	-----	Poisson's ratio, u_s	0.3
	-----	Modulus of Elasticity, E_s (N/mm^2)	200000
Plasticity	-----	Yield stress, f_y (N/mm^2)	500
	-----	Plastic Modulus, E_{sc} (N/mm^2)	2100

The behavior of the steel loading cylinder and supports under unidirectional loading was predicted using a bilinear stress-strain relationship. The Poisson ratio (v_s),

yield strength (f_y), tangent modulus (E_{sc}), and modulus of elasticity (E_s) must all be determined by the material model.

4.3 Constraints and interactions

The Multiple-Point Constraints (MPC) formulation was used in the ANSYS workbench to model the interaction between the beam surface and the steel plates and supports. Delineating the relationship between the two surfaces allowed for this to be achieved. As shown in Fig. 28, the no-separation type was chosen.

4.4 Boundary conditions and loads

According to Fig. 28, the beam was loaded using a load control system that applied force through the steel loading plate, gradually increasing the load by 0.4 kN at each stage. The boundary conditions of the beam were considered simply supported.

4.5 Type of analysis and outcomes

ANSYS static structural analysis was performed on every circumstance in this investigation. ANSYS solves nonlinear problems using Newton-Raphson. Material nonlinearity causes the current investigation nonlinear. Form nonlinearity was disregarded. Our investigation yielded critical strain, force reaction, and stress data.

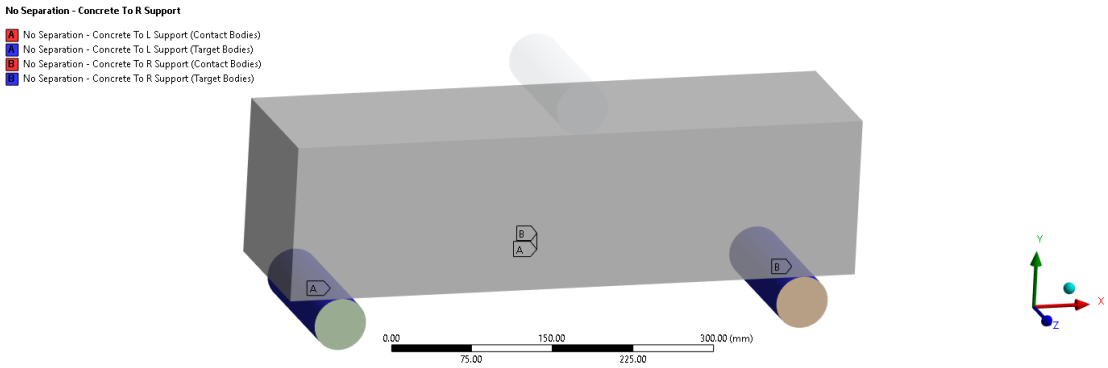

a) Interaction between LWFRC beams and supports

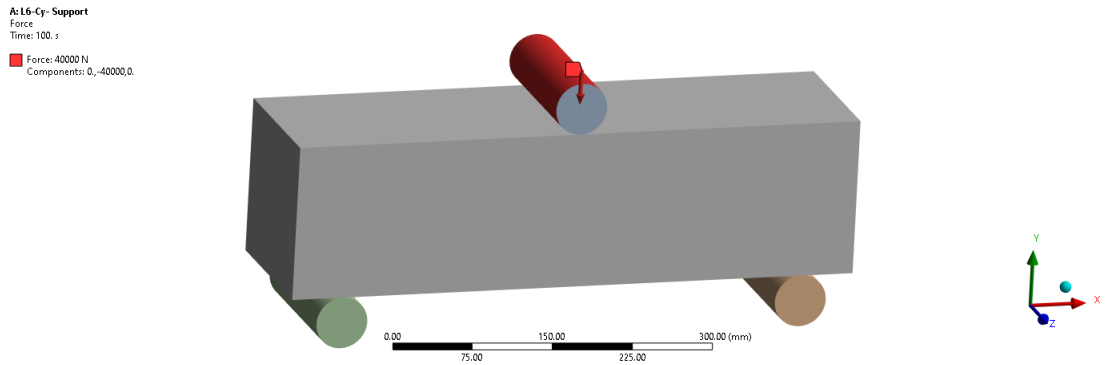

b) Loading

Fig. 28: Interaction and Loading of LWFRC beams.

4.6 Validation and Results of FEM

The maximum loads and flexural tensile strengths for every LWFRC beam are listed in Table 9. Comparing the outcomes of multiple specimens demonstrates how various conditions impact the intended beams' performance. It closely looks at and contrasts the finite element method (FEM) results with the experimental findings.

Table 9: The experimental and finite element model results of the LWFRC beams examined in the current study.

Group	Mix	Ultimate load; P_u (kN)			Modulus of rupture; f_{ctr} (N/mm^2)		
		(A) Experimental	(B) FEM	(A) / (B)	(C) Experimental	(D) FEM	(C) / (D)
Group1	D12C	7.75	8.00	0.97	1.55	1.60	0.97
	D12F	8.25	8.40	0.98	1.65	1.64	1.01
	D12S	8.50	8.80	0.97	1.70	1.76	0.97
Group2	D15C	15.00	15.20	0.99	3.00	3.04	0.99
	D15F	16.00	16.40odel	0.98	3.20	3.28	0.98
	D15S	17.00	17.20	0.99	3.40	3.44	0.99

Group3	**D18C**	25.00	25.20	0.99	5.00	5.04	0.99
	D18F	25.50	25.60	1.00	5.10	5.12	1.00
	D18S	26.50	26.80	0.99	5.30	5.36	0.99
Mean							0.985
STD							0.013
COV %							1.324
R^2							0.9997

Table 9 presents the ultimate loads (P_u) and modulus of rupture (f_{ctr}) values for each LWFRC beam examined in this study. The results indicate that the FEM analysis precisely forecasted the ultimate loads for the evaluated LWFRC beams. The finite element method yields results approximately 0.99 times as effective as the experimental outcomes. It is essential to understand that all Finite Element Models (FEMs) operate in accordance with experimental behavior. The findings validate that the concrete modeling employed in the study was precise and beneficial.

The principal tensile total strains for the LWFRC beam D15S that was evaluated in this work are depicted in Fig. 29. Two different loading phases were used to measure these stresses. As an additional point of interest, the principal tensile plastic strain values and distribution for the LWFRC beam D15S investigated in this study at two different loading stages—0.75 Pu and Pu—are shown in Fig. 30. When seen from the tension surface, the primary tensile strains may be interpreted as representing the crack pattern and its width [2, 18, 66]. In addition, the findings demonstrate that the crack patterns generated by the FEM and the experimental data are compatible with one another.

Fig. 31 shows the normal strain distribution in the X-direction for the LWFRC beam D15S under investigation. The distribution is displayed at the 0.75 Pu and Pu loading stages. The maximum compression strain value was concentrated around the limits of the loading area at the upper top fiber of the beam, based on the distribution of the normal strain in the X-direction. The normal strain's conduct served as evidence for this. During this time, the bottom fiber under the load position—which was situated in the center of the beam's span—was discovered to have the highest tensile strain value.

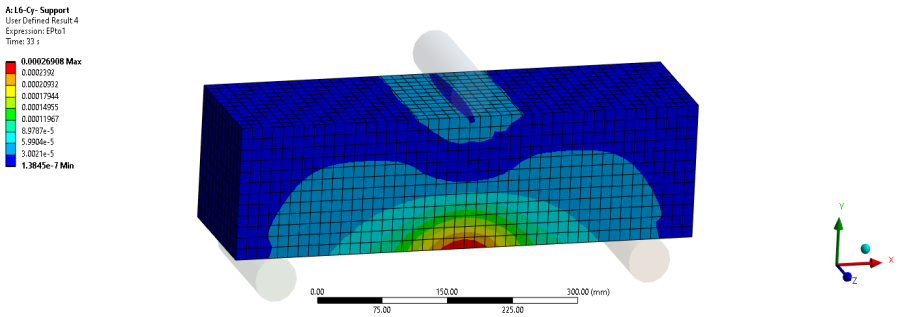

a) P= 0.75 P_u

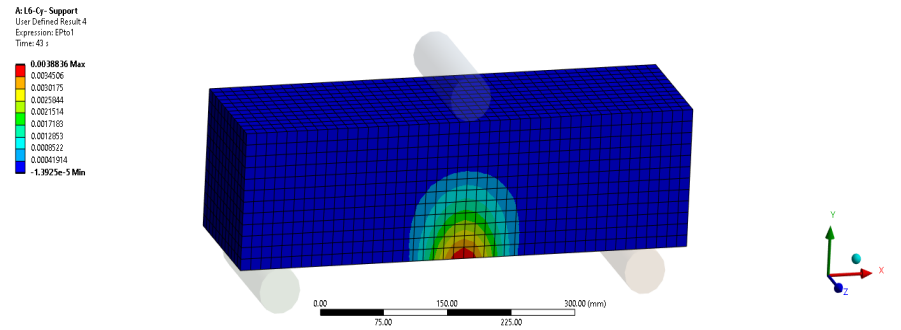

b) P= P_u

Fig. 29: The LWFRC specimen D15S's principal tensile strain at various load stages.

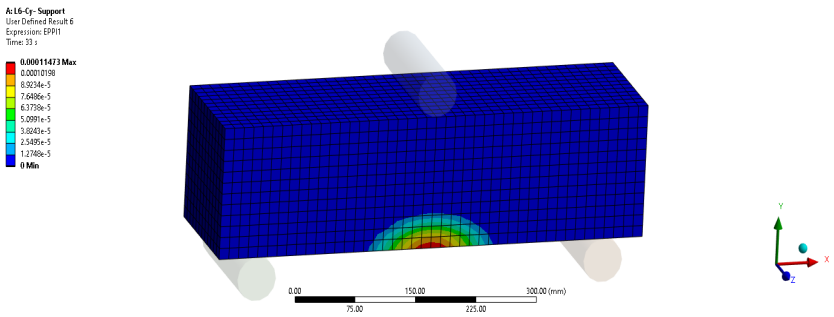

a) P= 0.75 P_u

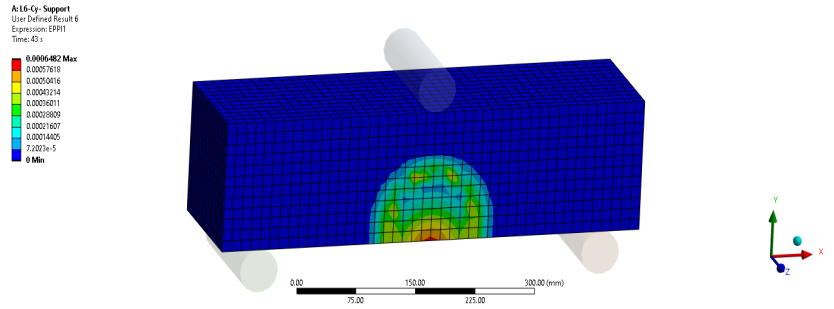

b) P= P_u

Fig. 30: The plastic principal tensile strain for LWFRC specimen D15S at different load levels.

The LWFRC specimen D15S that was examined in this investigation at two distinct loading stages—0.75 Pu and Pu—shows the usual stress values in the X-direction in Fig. 32. Two distinct loading phases existed.

The upper top fiber of the beam's maximum compression stress value was limited to the loading area's boundaries based on the distribution of normal stress in the X-direction. The loaded state of the beam served as evidence for this. During this time, the bottom fiber in the mid-span of the beam had the highest tensile stress value. At the load position, all of this happened at once. Additionally, as Fig. 32 illustrates, the microplane model's impact of damage was evident in the stress distribution along the beam span, namely in the tensile bottom fibers. In the microplane model, this was especially apparent.

Fig. 33 shows the ultimate load judgment from the FEM and the experimental results for the LWFRC specimens used in this investigation. The average value of the experimental ultimate load to the FEM ultimate load was 0.985, as seen in both Fig. 33 and Table 9. Furthermore, the coefficient of variation (COV) and coefficient of determination (R^2) were 1.324% and 0.9997, respectively, and the standard deviation (STD) was 0.013. The table contains each of these values.

The results of the finite element method (FEM) reveal that the microplane model effectively predicts the flexural behavior of lightweight fiber reinforced concrete (LWFRC) beams reinforced with hybrid fibers (steel and polypropylene) and lightweight aggregates, such as EPS or Perlite.

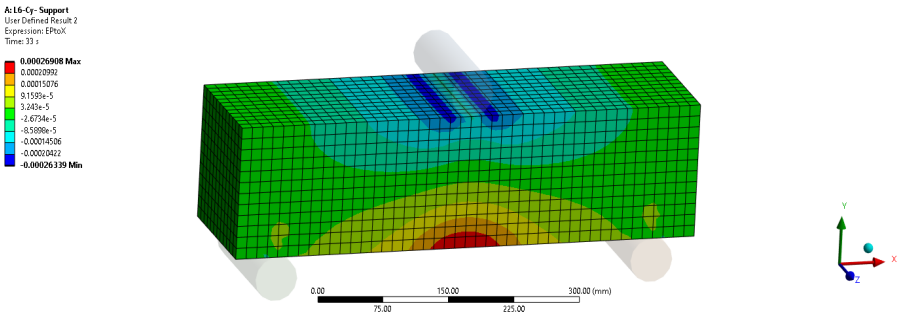

a) P= 0.75 P_u

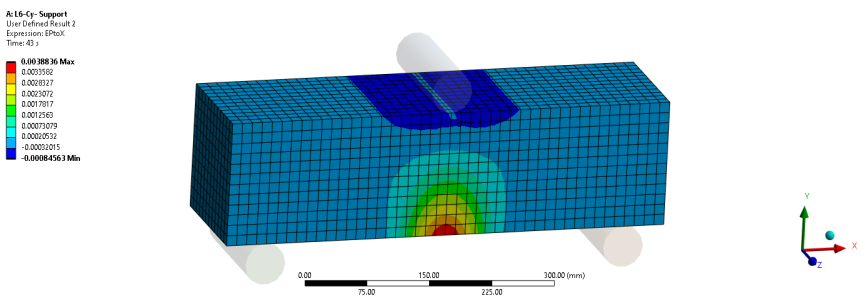

b) P= P_u

Fig. 31: The normal strain for LWFRC specimen D15S in the X-direction at various load levels.

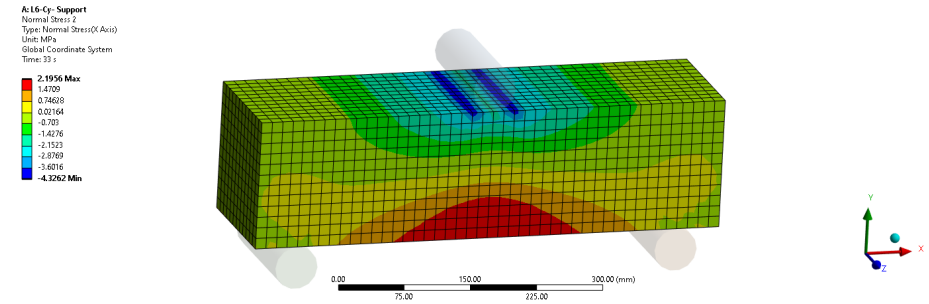

a) P= 0.75 P_u

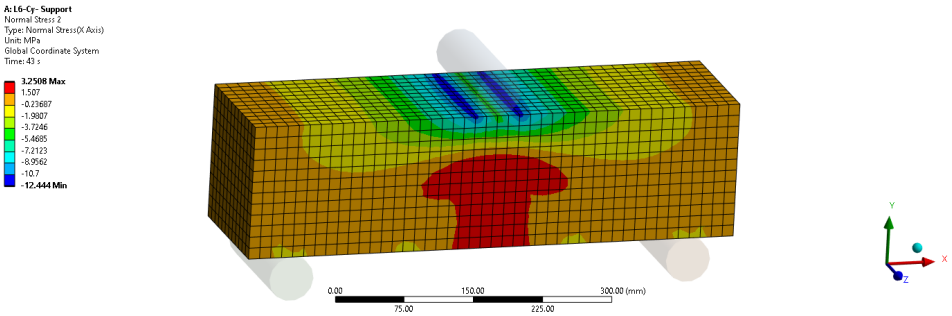

b) P= P_u

Fig. 32: LWFRC specimen D15S's normal stress in the X-direction at various load levels.

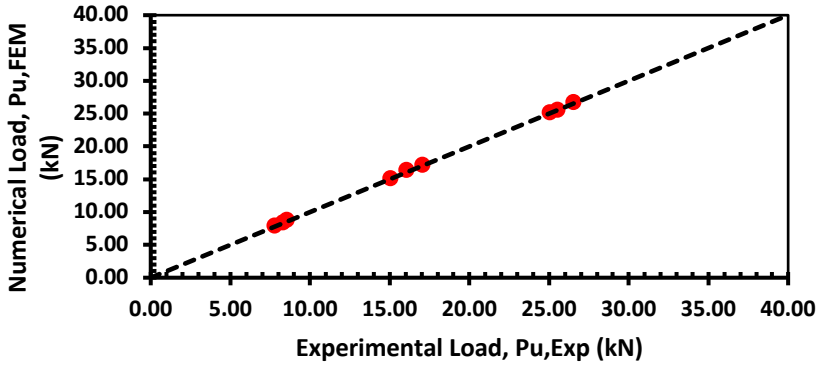

Fig. 33: Comparison between the experimental and FEM ultimate load results.

This conclusion is reached after comparing the FEM results to the experimental outcomes. Using the ANSYS finite element program, a numerical study could be carried out on LWFRC beams in order to investigate the structural behavior of large-scale elements. This would result in a reduction of the substantial costs that are associated with experimental programs for large-scale LWFRC beams that incorporate hybrid fibers with lightweight aggregates, such as EPS or Perlite.

5. The Effect of Utilizing LWFRC on the Economy

Despite EPS or perlite being comparatively costly relative to normal-weight aggregate, their advantageous attributes, including diminished density that may result in reduced design dimensions, must be acknowledged in the economic assessment. The ultimate bending moment, Mu, for a standard reinforced concrete section utilizing LWFRC is calculated based on the force equilibrium in the cross-section illustrated in Fig. 34, as per Eqs. 11 to 17. Fig. 34 presents a schematic representation of a segment of a LWFRC beam, contrastingly illustrating the real distribution of normal stresses. Furthermore, the simplified idealized distribution of normal stresses in the LIWFRC cracked section, as proposed by Yasin et al., [66], is illustrated Fig. 34.

According to Fig. 34 and due to the equilibrium:

$$c = 1.25a \qquad \text{(Eq. 11)}$$

$$C = T \qquad where;\ T = T_f + T_s \qquad \text{(Eq. 12)}$$

$$C = 0.67 \times \frac{f_{cu}}{\gamma_c} \times b \times a \qquad \text{(Eq. 13)}$$

$$T_f = \frac{f_t}{\gamma_t} \times b \times (h - 1.25a) \qquad \text{(Eq. 14)}$$

$$T_s = A_s \times \frac{f_y}{\gamma_s} \qquad \text{(Eq. 15)}$$

$$a = \frac{(A_s \times \frac{f_y}{\gamma_s} + \frac{f_t}{\gamma_t} \times h \times b)}{b \times (0.67 \times \frac{f_{cu}}{\gamma_c} + 1.25 \times \frac{f_t}{\gamma_t})} \qquad \text{(Eq. 16)}$$

$$M_u = T_f \times (0.5 \times h - 0.125 \times a) + T_s \times \left(d - \frac{a}{2}\right) \qquad \text{(Eq. 17)}$$

Where:

f_{cu} = 28-day cube compressive strength of LWFRC (MPa); f_t = uniaxial tensile strength of LWFRC (MPa), which can be approximated as 0.67 times the splitting tensile strength, fsp, as proposed by Shoukry et al., [73]; fy = yield strength of steel reinforcement (MPa); d = effective depth of tension steel (mm); h = beam thickness (mm); b = beam width (mm); a = depth of the compression stress block (mm); γ_c = material reduction factor for concrete under compression (1.5); γ_t = material reduction factor for concrete under tension (2.0); γ_s = material reduction factor for steel reinforcement (1.15); M_u = ultimate moment (N.mm). It is important to highlight that in this study, all material reduction factors are assigned a value of one when the proposed equation is applied.

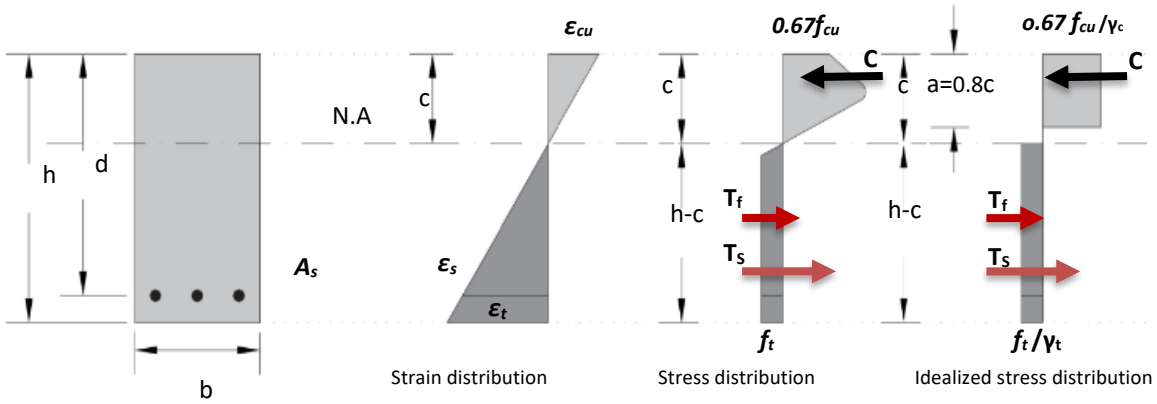

Fig. 34: Schematic illustrations of strain and theoretical stress distributions of LWFRC derived from the proposed calculations

To determine the expected ultimate moment for various LWFRC mixes, investigate the effects of EPS and perlite on flexural behavior, and compare it with the ultimate moment of an RC beam made from regular normal strength concrete, this study used a beam measuring 120 x 300 x 3000 mm, reinforced with 2T16, and two branch stirrups spaced 200 mm apart. The ultimate moment of the LWFRC beams in group 1 (D12C, D12F, and D12S) is about equivalent to 38% to 40% of the NSC beam's ultimate moment (RN). In contrast, the ultimate moment of the LWFRC beams in group 2 (D15C, D15F, and D15S) is roughly 82% to 87% of the NSC beam's ultimate moment (RN). The final moment, however, rose by roughly 21, 22, and 23% for LWFRC beams D18C, D18F, and D18S, respectively, for LWFRC beams in group 3, as given in Table 10.

Although EPS or perlite is relatively expensive compared to normal-weight aggregate, their potential benefits, such as reduced density, which could lead to lower design dimensions, cannot be ignored in the economic analysis.

Reduced density is one advantage of employing EPS or perlite as a lightweight aggregate; this can result in a thinner design sections or less reinforcement for the LWFRC beam. A cost-benefit analysis of each mix should be conducted, taking into account the material cost reductions coming from increases in strength per unit volume, as EPS or perlite is more costly than normal-weight aggregate. This was accomplished by calculating the cost of the LWFRC beam per unit length; the analysis's findings are shown in Table 11.

Table 10: Ultimate moment of the LWFRC beams.

Beam	Dimensions (mm)			Reinforcement*	a (mm)	Check		M_u (kN.m)	M_u /M_u (RN)
	b	h	d			C (kN)	T (kN)		
RN	120	300	262	2 T 16	80.02	160.850	160.850	**35.71**	**1.00**
D12C					209.31	84.817	84.817	**13.41**	**0.38**
D12F					209.46	87.273	87.273	**13.79**	**0.39**
D12S					209.20	89.779	89.779	**14.20**	**0.40**
D15C					189.73	174.237	174.237	**29.21**	**0.82**
D15F					182.62	176.194	176.194	**30.11**	**0.84**
D15S					175.54	178.640	178.640	**31.08**	**0.87**
D18C					105.95	219.734	219.734	**43.23**	**1.21**
D18F					106.18	221.004	221.004	**43.42**	**1.22**
D18S					106.14	223.689	223.689	**43.87**	**1.23**

*f_y= 400 (MPa)

The results of Tables 10 and 11 indicate that selecting EPS and perlite with a volume content of 50% in group 1 yields the lowest flexural strength of the LWFRC mix compared to an RC beam formed from normal-weight concrete, and that it also shows a high relative cost. On the other hand, selecting EPS and perlite with a volume content of 40% in group 2 cannot significantly improve the flexural strength of the LWFRC mix compared to an RC beam formed from normal-weight concrete, and it shows the highest relative cost. Finally, using EPS with a volume content of 30% in group 3 can significantly improve the flexural strength of the LWFRC mix compared to an RC beam formed from normal-weight concrete and yield the lowest relative cost among the groups.

Table 11: The total cost of the LWFRC beams per unit length.

Beam	Dimensions (mm)			Reinforcement*	Cost (EGP/unit length of the beam)**			Relative cost
	b	h	d		Cost of mix	Cost of Rft	Total cost	
RN	120	300	262	2 T 16	114.19	360.00	**474.19**	**1.00**
D12C					306.97		**666.97**	**1.41**
D12F					389.77		**749.77**	**1.58**
D12S					344.77		**704.77**	**1.49**
D15C					351.97		**711.97**	**1.50**
D15F					434.77		**794.77**	**1.68**
D15S					389.77		**749.77**	**1.58**
D18C					264.78		**624.78**	**1.32**
D18F					347.58		**707.58**	**1.49**
D18S					302.58		**662.58**	**1.40**

*f_y= 400 (MPa), and **1.00 USD ≈ 50.00 EGP

LWFRC mixes in groups 1 and 2, with densities of 1200 and 1500 kg/m3, are unable to lower the cost or design thickness of the beam because of flexure, according to the cost data shown in Table 11. However, because their end product mix is less expensive than the other LWFRC mixes, the LWFRC combinations in group 3 exhibit lower relative costs. It should be mentioned that employing EPS at 30% volume in the LWFRC mix could result in the

lowest relative cost when compared to the reference beam in the event that the concrete sections of the beam fail due to compression, shear, or torsion, which calls for more experimental research.

6. Conclusion

This extensive experimental and numerical study effectively established the feasibility of producing lightweight fibre-reinforced concrete (LWFRC) using hybrid steel and polypropylene fibres, along with EPS and perlite aggregates sourced from local Egyptian materials, across a broad density spectrum (1200-1800 kg/m³). The research offers essential insights into material behavior, prediction relationships, non-destructive testing calibration, numerical modeling validation, and economic factors. According to this study, the main findings and conclusions are encapsulated as follows:

1. All LWFRC mixtures exhibited very low workability (slump < 50 mm, class S1 according to EN 206:2013) due to the combined effects of EPS, perlite, and hybrid fiber content. The slump values ranged from 30 mm for the lowest-density mixes (Group 1) to 45 mm for the highest-density mixes (Group 3), demonstrating that EPS and perlite content significantly reduce workability.
2. The experiment showed that for all combinations of LWFRC, there was a strong linear connection (R2 = 0.9972) between the densities of freshly mixed concrete and hardened concrete after 28 days. This allowed for more accurate quality control during production since there was no longer any need to wait for the curing process to finish. By being able to predict the future, we can change the amount of each ingredient used throughout production to meet the design requirements.
3. Three separate density categories were produced by painstakingly adjusting the EPS and perlite contents; these categories exhibited different mechanical characteristics. Group 1, which accounts for half of the lightweight aggregate volume and has a density of about 1200 kg/m³, achieved compressive strengths between 5.04 and 5.34 MPa. This means that the concrete is very lightweight and may be used for tasks where strength is not the main issue. Group 2, which makes up 40% of the lightweight aggregate volume and has a density of about 1500 kg/m³, has compressive strengths ranging from 11.42 to 12.66 MPa. This is almost twice as powerful as Group 1. Group 3, which was over five times stronger than Group 1, achieved structural-grade compressive strengths ranging from 25.80 to 26.21 MPa with a 30% EPS content free of perlite and a density of around 1800 kg/m³. But compared to regular weight concrete, its density was 24–28% lower.
4. According to experimental test results, second-order polynomial relationships ($R^2 > 0.96$) were developed relating density to compressive strength, splitting tensile strength, and flexural tensile strength, providing reliable tools for predicting mechanical properties based solely on LWFRC density.
5. Partial replacement of cement with supplementary materials (fly ash or silica fume at 50 kg/m³) consistently enhanced compressive strength across all density groups, with silica fume demonstrating superior performance. Specimens D12S, D15S, and D18S (containing silica fume) exhibited the highest compressive strengths within their respective density groups, validating the pozzolanic contribution to matrix densification and interfacial bond improvement.
6. The cylinder-to-cube strength ratio (f_c'/f_{cu}) remained relatively constant at approximately 0.85-0.90 across all LWFRC mixtures, consistent with the conversion factor proposed by ECP 203-2025 for normal-weight concrete, indicating that this fundamental relationship is preserved in LWFRC systems.
7. The splitting tensile strength increased from 1.10 MPa to 4.67 MPa (325% improvement), while flexural tensile strength rose from 1.55 MPa to 5.30 MPa (242% improvement) as density increased from 1200 to 1800 kg/m³. The hybrid fiber system (1% total volume: 0.5% steel + 0.5% polypropylene) effectively bridged microcracks and enhanced ductility across all density levels.
8. The normalized strength ratios $f_{sp}/\sqrt{f_{cu}}$ (ranging from 0.55 to 0.91) and $f_{ctr}/\sqrt{f_{cu}}$ (ranging from 0.72 to 1.04) exceeded the values proposed by ECP 203-2025 for normal-weight concrete (0.42 and 0.60, respectively), demonstrating the beneficial effect of hybrid fiber reinforcement in enhancing tensile capacity and ductility in LWFRC systems.
9. For all LWFRC mixes, the ratio f_{sp}/f_{ctr} ranged from 0.73 to 0.88, higher than the value (0.70) proposed by ECP 203-2025 for normal weight concrete without fibers, indicating enhanced flexural performance relative to splitting tensile strength in fiber-reinforced systems.
10. Customized Schmidt hammer calibration curves were successfully developed for LWFRC with high accuracy ($R^2 > 0.92$) across three measurement orientations. Direction-dependent second-order polynomial equations for compressive strength prediction were established for downward, horizontal, and upward orientations. Additionally, a calibration curve for splitting tensile strength prediction was developed, enabling rapid, non-destructive assessment of tensile capacity. These calibration curves differ significantly from standard Schmidt hammer correlations for normal-weight concrete,

emphasizing the necessity of mixture-specific calibrations for LWFRC to avoid substantial errors in strength estimation.

11. The coupled damage-plasticity microplane model implemented in ANSYS Workbench 2023 R2 demonstrated exceptional accuracy in predicting ultimate loads and flexural behavior of LWFRC beams. The mean experimental-to-FEM ratio was 0.985 with a coefficient of determination $R^2 = 0.9997$ and coefficient of variation COV = 1.324%, indicating excellent agreement across all nine mixture designs. The model successfully captured crack patterns, stress distributions, strain profiles, and failure modes, validating its applicability for design optimization and parametric studies of LWFRC structural elements.
12. Cost analysis revealed that EPS is more cost-effective than perlite for achieving weight reduction, as higher perlite content in Group 2 led to disproportionate cost increases without corresponding benefits. The study established that LWFRC with a density of 1800 kg/m³ can achieve structural-grade compressive strengths (≈27 MPa) while maintaining significant benefits, including reduced dead load (24-28% weight reduction), improved thermal insulation, and enhanced ductility through hybrid fibre reinforcement.

Conflict of interest

None.

Acknowledgments

We would like to express our deepest gratitude to [Department of Structural Engineering, Faculty of Engineering, Alexandria University, Egypt] for the immense help in executing the experimental part of the research. We also have to thank Prof. Dr. Mohamed Ahmed Hafez; Associate Professor of Dam Engineering and to [INTI-IU-Malaysia] for the generous support through the research grant [INTI-FEQS-01-06-2023].

Declaration of generative AI and AI-assisted technologies in the manuscript preparation process

During the preparation of this work, the author(s) used [https://www.perplexity.ai/ perplexity Pro] in order to [cover the previous studies in the introduction and the novelty of the study]. After using this tool/service, the authors reviewed and edited the content as needed and take full responsibility for the content of the published article.

References

[1] M.A. Elnaggar, M.S. Omar, A.M. Yassin, Rehabilitation of defective connections between two precast concrete segments (experimental and analytical study), Construction and Building Materials 368 (2023).

[2] A.M. Yassin, M.M. Eldin, M.S. Omar, M.A. Hafez, M.A. Elnaggar, Effect of nano-silica on the flexural behavior and mechanical properties of self-compacted high-performance concrete (SCHPC) produced by cement CEM II/A-P (experimental and numerical study), Case Studies in Construction Materials 21 (2024).

[3] I.A. Ja'e, Z.C. Muda, H. Almujibah, C.V. Amaechi, A. Syamsir, U.J. Alengaram, A.E.A. Elshekh, M.O. Bashir, Structural impact resilience of lightweight fiber-reinforced LECA concrete using ANN and RSM technique, Construction and Building Materials 471 (2025).

[4] I.A. Ja'e, Z.C. Muda, A. Syamsir, C.V. Amaechi, H. Almujibah, A.E.A. Elshekh, M.O. Bashir, A.H. Almaliki, Structural performance of lightweight fibre-reinforced oil palm shell concrete subjected to impact loadings under varying boundary conditions, Case Studies in Construction Materials 22 (2025).

[5] ACI Committee 318, Building Code Requirements for Structural Concrete (ACI 318-25), American Concrete Institute, Farmington Hills, MI 48331, USA, 2025.

[6] R.K. Rakaa, R.M. Abbas, Mechanical Properties of Lightweight EPS Self-compacting Concrete Reinforced with Steel Fibers, Journal of Engineering 30(06) (2024) 125-140.

[7] H. Li, Y. Wei, K. Meng, L. Zhao, B. Zhu, B. Wei, Mechanical properties and stress-strain relationship of surface-treated bamboo fiber reinforced lightweight aggregate concrete, Construction and Building Materials 424 (2024).

[8] M. Al-Daraji, N. Aljalawi, The Effect of Kevlar Fibers on the Mechanical Properties of Lightweight Perlite Concrete, Engineering, Technology & Applied Science Research 14(1) (2024) 12906-12910.

[9] N. Zanjad, C. Nayak, S. Pawar, S. Naik, Experimental Analysis of Mechanical Properties of Fiber Reinforced Cenosphere Lightweight Concrete with Higher Temperature Effect, Communications on Applied Nonlinear Analysis 31(1) (2024).

[10] M. Abid, G.Q. Waqar, J. Mao, M.F. Javed, H. Almujibah, Mechanical properties, microstructure and GEP-based modeling of basalt fiber reinforced lightweight high-strength concrete containing SCMs, Journal of Building Engineering 96 (2024).

[11] A.S. Najim, S. Beddu, Z. Itam, Enhancing Mechanical Properties of Fiber-Reinforced Self-Compacting Geopolymer Concrete Using Lightweight Aggregate, Annales de Chimie -

Science des Matériaux 48(5) (2024) 699-707.

[12] H. Moradi, S.A.H. Hashemi, Neural predictional of Mechanical Properties of Fiber-Reinforced Lightweight Concrete Containing Metakaolin at High Temperatures, Proceedings of the 9th International Conference on Civil, Structural and Transportation Engineering (ICCSTE 2024), 2024.

[13] S.A. Stel'makh, E.M. Shcherban, A.N. Beskopylny, L.R. Mailyan, B. Meskhi, I. Razveeva, A. Kozhakin, N. Beskopylny, Prediction of Mechanical Properties of Highly Functional Lightweight Fiber-Reinforced Concrete Based on Deep Neural Network and Ensemble Regression Trees Methods, Materials (Basel) 15(19) (2022).

[14] J. Wei, Q. Yang, Q. Jiang, X. Li, S. Liu, K. Li, Q. Wang, Mechanical properties of basalt fiber reinforced ambient-cured lightweight expanded polystyrene geopolymer concrete, Journal of Building Engineering 80 (2023).

[15] A.S. Najim, S. Beddu, Z. Itam, Mechanical Properties of Fiber-Reinforced Self-Compacting Geopolymer Concrete Using Lightweight Aggregate under Microwave Curing Condition, Journal of Building Material Science 7(3) (2025).

[16] H. WEI, M. XIN-WEI, S. YU-JIAO, R. SHANSHAN, Study on the Mechanical Properties and Damage Constitutive Model of Hybrid Fibre-Reinforced EPS Lightweight Aggregate Concrete, Tehnicki vjesnik - Technical Gazette 27(6) (2020).

[17] D. Barnat-Hunek, J. Gora, W. Andrzejuk, G. Lagod, The Microstructure-Mechanical Properties of Hybrid Fibres-Reinforced Self-Compacting Lightweight Concrete with Perlite Aggregate, Materials (Basel) 11(7) (2018).

[18] A.M. Yassin, M.A. Hafez, M.G. Aboelhassan, Experimental and Numerical Investigation on the Effect of Different Types of Synthetic Fibers on the Flexure Behavior and Mechanical Properties of 3D Cementitious Composite Printing Provided with Cement CEM II/A-P, Buildings 15(7) (2025).

[19] F. Jiang, W. Deng, Q. Wang, J. Wang, Z. Mao, Performance Research and Engineering Application of Fiber-Reinforced Lightweight Aggregate Concrete, Materials (Basel) 17(22) (2024).

[20] H. Wei, T. Wu, X. Yang, Properties of Lightweight Aggregate Concrete Reinforced with Carbon and/or Polypropylene Fibers, Materials (Basel) 13(3) (2020).

[21] M. Kadela, M. Malek, M. Jackowski, M. Kunikowski, A. Klimek, D. Dudek, M. Roskowicz, Recycling of Tire-Derived Fiber: The Contribution of Steel Cord on the Properties of Lightweight Concrete Based on Perlite Aggregate, Materials (Basel) 16(5) (2023).

[22] R.M. Abbas, R.K. Rakaa, Structural Performance of Lightweight Fiber Reinforced Polystyrene Aggregate Self-Compacted Concrete Beams, Engineering, Technology & Applied Science Research 13(5) (2023) 11865-11870.

[23] A.S. Salah Alden, A.I. Al-Hadethi, The Influence of Waste Plastic Fiber on the Characteristics of Light Weight Concrete with Expanded Polystyrene (EPS) as Aggregate, Journal of Engineering 29(08) (2023) 16-26.

[24] A.I. Al-Hadithi, N.N. Hilal, M. Al-Gburi, A.H. Midher, Structural behavior of reinforced lightweight self-compacting concrete beams using expanded polystyrene as coarse aggregate and containing polyethylene terephthalate fibers, Structural Concrete 24(5) (2023) 5808-5826.

[25] Y. Sun, C. Li, J. You, C. Bu, L. Yu, Z. Yan, X. Liu, Y. Zhang, X. Chen, An Investigation of the Properties of Expanded Polystyrene Concrete with Fibers Based on an Orthogonal Experimental Design, Materials (Basel) 15(3) (2022).

[26] C.T. Dang, M. Pham, N.H. Dinh, Experimental Study on Compressive and Flexural Performance of Lightweight Cement-Based Composites Reinforced with Hybrid Short Fibers, Materials (Basel) 16(12) (2023).

[27] V. Lusis, K.K. Annamaneni, A. Krasnikovs, Concrete Reinforced by Hybrid Mix of Short Fibers under Bending, Fibers 10(2) (2022).

[28] S.A. Stel'makh, E.M. Shcherban, A. Beskopylny, L.R. Mailyan, B. Meskhi, V. Varavka, Quantitative and Qualitative Aspects of Composite Action of Concrete and Dispersion-Reinforcing Fiber, Polymers (Basel) 14(4) (2022).

[29] H.H.Z. Khalel, M. Khan, Modelling Fibre-Reinforced Concrete for Predicting Optimal Mechanical Properties, Materials (Basel) 16(10) (2023).

[30] H.H.Z. Khalel, M. Khan, A. Starr, N. Sadawi, O.A. Mohamed, A. Khalil, M. Esaker, Parametric study for optimizing fiber-reinforced concrete properties, Structural Concrete 26(1) (2024) 88-110.

[31] A.A. Abd, R.M. Abbas, Residual Strength of Fiber-reinforced EPS Lightweight Concrete After Exposure to Fire, Engineering, Technology & Applied Science Research 15(5) (2025) 26587-26593.

[32] S. Widodo, Bond Strength between Hybrid Fiber-Reinforced Lightweight Aggregate Concrete Substrate and Self-Compacting Concrete as Topping Layer, Advances in Civil Engineering 2017 (2017)

1-9.

[33] Fédération Internationale du Béton (fib), Lightweight Aggregate Concrete, fib bulletin 4, 1999.

[34] Fédération Internationale du Béton (fib), Lightweight Aggregate Concrete, fib bulletin 8, 2000.

[35] ACI Committee 213, Guide for Structural Lightweight-Aggregate Concrete, ACI 213R-14, American Concrete Institute, USA, 2014.

[36] European Committee for Standardization, Eurocode 2: Design of Concrete Structures : Part 1-1: General Rules and Rules for Buildings, European Committee for Standardization2004.

[37] BSI, BS 8500-1:2015+A2:2019: Concrete – Complementary British Standard to BS EN 206, BSI, London, UK, 2019.

[38] Fédération Internationale du Béton (fib), fib model code for concrete structures 2020, Fédération Internationale du Béton (fib), Lausanne, Switzerland, 2024.

[39] JSCE No.15, STANDARD SPECIFICATIONS FOR CONCRETE STRUCTURES 2007 "Design", Japan Society of Civil Engineers (JSCE), Yotsuya 1-chome, Shinjuku-ku, Tokyo 160-0004, JAPAN, 2007.

[40] The Housing and Building National Research Center (HBRC), Egyptian Code for Design and Construction of Reinforced Concrete Structures, ECP 203-2025, Egyptian Code committee for Design and Construction of Reinforced Concrete Structures, Egypt, 2025.

[41] C.I.N.R.C. CNR-DT, Rome, 204/2006 Guide for the design and construction of fiber-reinforced concrete structures, (2006).

[42] AFGC, ULTRA HIGH PERFORMANCE FIBRE-REINFORCED, Recommendations, AFGC, Association Française de Génie Civil, france, 2013.

[43] JSCE No.82, Recommendations for design and construction of High Performance Fiber Reinforced Cement Composites with multiple fine cracks (HPFRCC), Japan Society of Civil Engineers, Concrete Committee, Japan, 2008.

[44] ACI Committee 544, Guide to Design with Fiber-Reinforced Concrete, ACI 544.4R-18, American Concrete Institute Farmington Hills, MI 48331, USA, 2018, p. 39.

[45] B.A. Alazzam, M. Alkhatib, K. Shaalan, Artificial Intelligence Chatbots: A Survey of Classical versus Deep Machine Learning Techniques, Information Sciences Letters 12(4) (2023) 1217-1233.

[46] T.V. Montshiwa, T. Botlhoko, Modelling and Predicting Learners Numeracy Test Results using Some Regression and Machine Learning Classifiers, Journal of Statistics Applications & Probability 12(3) (2023) 1345-1363.

[47] R. Alazaidah, A. Al-Shaikh, M.R. AL-Mousa, H. Khafajah, G. Samara, M. Alzyoud, N. Al-Shanableh, S. Almatarneh, Website Phishing Detection Using Machine Learning Techniques, Journal of Statistics Applications & Probability 13(1) (2024) 119-129.

[48] S.A. Alomari, Skin Cancer and Benign Lesion Classification Using Machine Learning Algorithms, Applied Mathematics & Information Sciences 19(5) (2025) 1093-1107.

[49] M.R. Girgis, A.M. Zaki, E. Elgeldawi, M.M. Abdallah, A.A. Ahmed, MACT: A Novel Framework for Automated Mobile Application Testing Using Machine Learning, Applied Mathematics & Information Sciences 19(5) (2025) 1079-1092.

[50] I.Y. Hamid, S.M.A. Yousif, S. Aljaloud, A.O.I. Abaker, H.Z.S. Elemam, K.A. Alruwaitee, M.I.A. Anja, Machine Learning Techniques in a Hybrid Forecasting Model for Oil Prices Combining ARIMA, Applied Mathematics & Information Sciences 19(6) (2025) 1241-1252.

[51] Y. N., S.I.S. Mohammad, N. Raja, R.R.H. S., K.H. S., A.R. N., A. Vasudevan, M.F.A. Hunitie, N. Alshdaifat, Mathematical Formulation of Fuzzy Grammar in English Syntax and Morphology, Applied Mathematics & Information Sciences 19(5) (2025) 1049-1065.

[52] A.Shoiynbek, D. Kuanyshbay, P. Menezes, G. Assunc¸ao, B. Meraliyev, A. Mukhametzhanov, T. Shoiynbek, S. Sklyar, The Automated Method of Collecting and Labeling Data for Speech Emotion Recognition based on Face Emotion Recognition, Applied Mathematics & Information Sciences 19(5) (2025) 1067-1077.

[53] I.ANSYS, ANSYS Mechanical APDL 2023/R2 (Material Reference) ANSYS, Inc, (https://ansyshelp.ansys.com/public/account/secured?returnurl=/Views/Secured/corp/v242/en/ans_mat/ans_mat.html), USA, 2023.

[54] BSI, BS EN 206: 2013+ A1: 2016: Concrete. Specification, performance, production and conformity, BSI London, UK, 2013.

[55] ACI Committee 544, Report on Measuring Mechanical Properties of Hardened Fiber-Reinforced Concrete, ACI 544.9R-17, American Concrete Institute, 2017, p. 52.

[56] A.M. Yassin, M. Mohie Eldin, M.A. Hafez, M.A. Elnaggar, The Flexural Behavior and Mechanical Properties of Super High-Performance Concrete (SHPC) Reinforced Using the Hybridization of Micro Polypropylene and Macro Steel Fibers, Buildings 14(7) (2024).

[57] A.M. Yassin, M.M. Eldin, M.S. Omar, M.A. Hafez, M.A. Elnaggar, A new approach to calculate the shear strength of high-performance reinforced concrete beams fibered with micro polypropylene (experimental and analytical study), Engineering Structures 314 (2024).

[58] u.6zkana, O. Qoban, The hybrid effects of basalt and PVA fiber on properties of a cementitious composite: Physical properties and non-destructive tests, Construction and Building Materials 312(125292) (2021).

[59] H.M. Najm, O. Nanayakkara, M.M.S. Sabri, Destructive and Non-Destructive Evaluation of Fibre-Reinforced Concrete: A Comprehensive Study of Mechanical Properties, Materials (Basel) 15(13) (2022).

[60] A.A. Mohamad-Ali, M.D. Abdullah, A.H. Chkheiwer, Estimating Of Compressive Strength Of Different Types Of Concrete By Nondestructive Tests, 40th ISERD International Conference, Cairo, Egypt, 2016, pp. 29-36.

[61] D. Behera, K.Y. Liu, D. Gopalakrishnan, Experimental Prognostication of Ultra-High-Performance Lightweight Hybrid Fiber-Reinforced Concrete by Using Sintered Fly Ash Aggregate, Palm Oil Shell Aggregate, and Supplementary Cementitious Materials, Materials (Basel) 15(14) (2022).

[62] K. Sanchez, N. Tarranza, Reliability of Rebound Hammer Test in Concrete Compressive Strength Estimation, International Journal of Advances in Agricultural & Environmental Engineering 1(2) (2015).

[63] Y.S. Aksüt, M. Çullu, Ş. Yetgin, Modeling the Compressive Strength of Fiber–Reinforced Alkali-Activated Concrete Using Non-Destructive Methods in Short Curing Periods, Journal of Materials in Civil Engineering 37(11) (2025) 04025418.

[64] E.Tugrul Tunc, Relationship Between Schmidt Hammer Rebound Hardness Test and Concrete Strength Tests for Limestone Aggregate Concrete Based on Experimental and Statistical Study, Materials (Basel) 18(6) (2025).

[65] H.R. Kumavat, N.R. Chandak, I.T. Patil, Factors influencing the performance of rebound hammer used for non-destructive testing of concrete members: A review, Case Studies in Construction Materials 14 (2021).

[66] A.M. Yassin, M.A. Hafez, M. Mohie Eldin, The Flexural Behavior of Reinforced Ultra-High Performance Engineering Cementitious Composite (UHP-ECC) Beams Fabricated with Polyethylene Fiber (Numerical and Analytical Study), Buildings 14(11) (2024).

[67] Z.P. Bažant, P.G. Gambarova, Crack shear in concrete: Crack band microflane model, Journal of structural engineering 110(9) (1984) 2015-2035.

[68] Z.P. Bažant, B.H. Oh, Microplane model for progressive fracture of concrete and rock, Journal of Engineering Mechanics 111(4) (1985) 559-582.

[69] M. Leukart, E. Ramm, A comparison of damage models formulated on different material scales, Computational Materials Science 28(3-4) (2003) 749-762.

[70] I.Zreid, M. Kaliske, Regularization of microplane damage models using an implicit gradient enhancement, International Journal of Solids and Structures 51(19-20) (2014) 3480-3489.

[71] I.Zreid, M. Kaliske, An implicit gradient formulation for microplane Drucker-Prager plasticity, International Journal of Plasticity 83 (2016) 252-272.

[72] I.Zreid, M. Kaliske, A gradient enhanced plasticity–damage microplane model for concrete, Computational Mechanics 62(5) (2018) 1239-1257.

[73] M.E. Shoukry, A.M. Tarabia, A.M. Yassin, Punching shear strength of ultra-high-performance fibre concrete slab–column connections, Proceedings of the Institution of Civil Engineers - Structures and Buildings 175(8) (2022) 644-656.